

Infrared and Optical Spectroscopy of Type Ia Supernovae in the Nebular Phase

E.J.C. Bowers¹, W.P.S. Meikle¹, T.R. Geballe², N.A. Walton³, P.A. Pinto⁴,
V.S. Dhillon⁵, S.B. Howell⁶, M.K. Harrop-Allin⁷.

¹Astrophysics Group, Blackett Laboratory, Imperial College of Science, Technology and
Medicine, Prince Consort Road, London SW7 2BZ, UK

²Joint Astronomy Centre, 660 N. A'ohoku Place, University Park, Hilo, Hawaii 96720, USA

³Royal Greenwich Observatory, Apartado de Correos 321, 38780 Santa Cruz de La Palma,
Tenerife, Islas Canarias, Spain

⁴Steward Observatory, University of Arizona, Tucson, AZ 85721, USA

⁵Royal Greenwich Observatory, Madingley Road, Cambridge CB3 0EZ, UK

⁶Department of Physics and Astronomy, University of Wyoming, PO Box 3905, University
Station, Laramie, WY 82071, USA

⁷Mullard Space Science Laboratory, University College London, Holmbury St. Mary, Dork-
ing, Surrey, RH5 6NT, UK

Abstract

We present near-infrared (NIR) spectra for Type Ia supernovae at epochs of 13 to 338 days after maximum blue light. Some contemporary optical spectra are also shown. All the NIR spectra exhibit considerable structure throughout the J-, H- and K-bands. In particular they exhibit a flux ‘deficit’ in the J-band which persists as late as 175 days. This is responsible for the well-known red J-H colour. To identify the emission features and test the ^{56}Ni hypothesis for the explosion and subsequent light curve, we compare the NIR and optical nebular-phase data with a simple non-LTE nebular spectral model. We find that many of the spectral features are due to iron-group elements and that the J-band deficit is due to a lack of emission lines from species which dominate the rest of the IR/optical spectrum. Nevertheless, some emission is unaccounted for, possibly due to inaccuracies in the cobalt atomic data. For some supernovae, blueshifts of 1000–3000 km/s are seen in infrared and optical features at 3 months. We suggest this is due to clumping in the ejecta. The evolution of the cobalt/iron mass ratio indicates that ^{56}Co -decay dominates the abundances of these elements. The absolute masses of iron-group elements which we derive support the basic thermonuclear explosion scenario for Type Ia supernovae. A core-collapse origin is less consistent with our data.

Key words: stars: general - supernovae: general - infrared: stars.

1 Introduction

It is widely believed that the luminosity of a Type Ia supernova (SNIa) is due to the deposition of gamma-rays and positrons from the radioactive decay, $^{56}\text{Ni} \rightarrow ^{56}\text{Co} \rightarrow ^{56}\text{Fe}$, of ^{56}Ni created in the explosion (Pankey 1962; Colgate & McKee 1969). Given the central importance of this process it is surprising that only a couple of pieces of *direct* evidence in favour of a radioactively driven light curve have been presented. Axelrod (1980a,b) studied the [Co III] 0.59 μm feature in the Type Ia SN 1972E, and found that its decline was consistent with ^{56}Co decay. A similar result was obtained by Kuchner *et al.* (1994) who used optical spectra of a sample of Type Ia SNe to follow the Co/Fe mass ratio. Both of these studies made use of optical spectroscopy of Type Ia SNe in their ‘nebular’ or ‘late-time’ phase. By this, we mean the era starting about 60 days post-maximum-light when the ejecta are optically thin to most of the infrared (IR) and optical lines. (Throughout this paper, epochs are defined with respect to maximum light in the B-band, $t_{Bmax}=0$ days). Nevertheless, some of the stronger optical lines can remain optically-thick for a significant time after the nebular phase begins. Clumping can exacerbate this effect. In addition, the sheer number of strong lines in the optical region results in severe line blending, causing identification uncertainty and inaccurate flux measurement of individual lines. In particular, the identification and measurement of the [Co III] 0.59 μm line was vital for the work of Axelrod and Kuchner *et al.*. A concern about this identification was the extent of contamination by Na I D. Unfortunately, there are no other strong lines of Na I present in the optical spectra and so it was difficult to place an observational constraint on the strength of Na I D. Consequently, some doubt was expressed (Wheeler *et al.* 1993) as to the reliability of the 0.59 μm feature as a direct test of the radioactive decay model. However, as Kuchner *et al.* point out, it can be argued on theoretical grounds that significant Na I D contamination is unlikely.

Hoyle & Fowler (1960) proposed that a Type Ia supernova results from the explosion of a white dwarf due to the thermonuclear fusion to ^{56}Ni of $\sim 0.5\text{--}1 M_{\odot}$ of the nuclei suspended in the electron-degenerate gas. Different classes of models which invoke this mechanism are the Chandrasekhar-mass models (e.g. Iben & Tutukov 1984, Nomoto, Thielemann & Yokoi 1984; Khokhlov 1991; Woosley & Weaver 1994a) and sub-Chandrasekhar-mass models (Livne 1990; Livne & Glasner 1990; Woosley & Weaver 1994b; Livne & Arnett 1995; Höflich & Khokhlov 1995). While all these models tend to eject $0.2\text{--}1.0 M_{\odot}$ of ^{56}Ni , they nevertheless all have problems (Woosley & Weaver 1994b).

The thermonuclear explosion mechanism is challenged by S. Colgate and collaborators (Colgate *et al.* 1997). They favour instead a core-collapse model with low mass ejection ($<0.1 M_{\odot}$). The reason they advocate this hypothesis is due to apparent difficulties in accounting for the decline rates of the optical light curves at late times. As early as 100 days it is observed that the Type Ia BVR fluxes decline with a faster time-scale than the 77 day half-life of ^{56}Co . In both the thermonuclear and core-collapse scenarios, this can be initially explained as being due to an increasing fraction of the gamma-rays escaping

as the ejecta expand. Eventually, however, the luminosity is driven predominantly by the positrons which are more easily absorbed than the gamma-rays (positron emission occurs in 4% of the ^{56}Co decays). In the thermonuclear case, the large ejecta mass ($\sim 1 M_{\odot}$) means that the positrons continue to be totally trapped, even after they dominate the luminosity. The fact that the light curve nonetheless continues to decline faster than the ^{56}Co decay rate is explained as being due to an increasing fraction of the energy emerging at wavelengths longward of $2.5 \mu\text{m}$ and so escaping detection. In particular, strong fine-structure lines of [Fe II] and [Fe III] in the $15\text{--}30 \mu\text{m}$ range are anticipated (Axelrod, 1980). This crucial prediction has yet to be tested. As mentioned above, an alternative explanation is provided by the small ejecta mass ($\sim 0.1 M_{\odot}$) of the core-collapse model which results in a steadily increasing transparency to the positrons.

Clearly, it is vital to establish the mass of ^{56}Ni in the SN ejecta in order to distinguish between the thermonuclear and core-collapse explosion mechanisms. In particular, a conclusive test would be to determine the mass of iron in the ejecta at late times. Such a measurement also holds out the prospect of distinguishing between specific thermonuclear models, although higher precision is probably needed here. The measurement of the absolute mass of ejected iron is difficult and has rarely been attempted. Significant uncertainties exist in distance, atomic data, and ejecta conditions (ionization, temperature, density). The first attempts were by Meyerott (1980) and Axelrod (1980a,b) who inferred a substantial mass of ejected ^{56}Ni from the forbidden iron lines in the optical spectra of the Type Ia SN 1972E, although the aforementioned uncertainties meant that only a weak constraint on the mass ($0.3\text{--}1.0 M_{\odot}$) was achieved. More recently, Spyromilio *et al.* (1992) used near-infrared (NIR) and optical spectra of the *peculiar* Type Ia SN 1991T to deduce the presence of about $0.5 M_{\odot}$ of ^{56}Fe in the ejecta but also with a large uncertainty ($0.4\text{--}1.2 M_{\odot}$). Ruiz-Lapuente (1992) modelled the optical spectra of the *peculiar* Type Ia SN 1986G and derived a ^{56}Ni mass of about $0.4 M_{\odot}$, although this too was subject to large uncertainties in the atomic data used.

We conclude that the widespread belief in the standard Type Ia scenario of a thermonuclear explosion and radioactively-driven light curve rests on remarkably little direct evidence. In order to place our understanding of SNIas on a more secure observational basis we have begun a programme of NIR spectroscopy of a number of typical Type Ia supernovae during the nebular phase. Since the ejecta are optically thin, observation during this era offers the best prospects of measuring directly total relative and absolute masses. In the nebular phase we expect the ejecta to be cooled mainly through forbidden-line emission from singly- and doubly-ionized cobalt and iron atoms. Observation in the NIR region has a couple of advantages over the optical band. Optical lines are generally of higher excitation and so are more temperature-sensitive. In addition the opacity of certain optical transitions are higher than those in the IR, and may even be optically thick, especially if the ejecta are clumped. The presence of forbidden NIR lines of iron and cobalt in the Type Ia nebular-phase spectra together with the advent of sensitive IR spectrographs, and significant improvements in the accuracy of atomic data (Hummer *et al.* 1993), offers the possibility of a powerful direct test of both the explosion mechanism and of the radioactive decay hypothesis.

To test for the presence of radioactive cobalt we use forbidden cobalt and iron lines and a simple spectral synthesis model to determine both the total cobalt/iron mass *ratio* and the absolute masses of cobalt and iron over a sequence of epochs. The determination of absolute mass is, in principle, subject to greater uncertainty owing to its sensitivity to distance and temperature errors. The ratio method was applied originally to the Type II SN 1987A by Varani *et al.* (1990). The technique exploits several interesting features of the cobalt-iron nebula which render it relatively insensitive to the details of the spectral synthesis code. Firstly, the similar atomic configurations and thus excitation energies of iron and cobalt, plus the fact that if the iron and cobalt do arise from ^{56}Ni decay then they should be spatially co-extensive in the ejecta, means that estimates of the *ratios* of masses of Co^+/Fe^+ or $\text{Co}^{2+}/\text{Fe}^{2+}$ are much less sensitive to temperature or temperature gradients than are absolute mass determinations (Varani *et al.* 1990). Secondly, the first ionization potentials of iron and cobalt are virtually the same (7.9 eV for Fe and 7.87 eV for Co), and the second ionization potentials differ by only 5% (16.19 eV for Fe and 17.08 eV for Co) (Fuhr, Martin and Wiese 1988). Consequently the individual mass ratios Co^+/Fe^+ or $\text{Co}^{2+}/\text{Fe}^{2+}$ derived from model spectral matches to the data should be equal to the total cobalt/iron mass ratio. Thirdly, such ratios are largely unaffected by uncertainties in distance or extinction. This is particularly so for infrared lines where the extinction is lower.

Prior to this work, little was known about the NIR behaviour of Type Ia SNe in the nebular phase. NIR photometry in the 60–100 day era (Elias *et al.* 1981, 1985) revealed a strong flux-deficit in the J-band ($J-H \sim +1.5$). Indeed, this deficit was present as early as 15 days. The first NIR spectra of Type Ia SNe, *viz.* SN 1986G (Frogel *et al.* 1987; Graham *et al.* 1987) (published in Meikle *et al.* 1997), SN 1991T (Spyromilio, Pinto & Eastman 1994) and SN 1995D (Meikle *et al.* 1997) showed that the J–H reddening in the 13–60 day era is due to the presence of a deep, wide flux deficit between 1.1 and 1.5 μm . This deficit, originally suggested to be a broad absorption (Kirshner *et al.* 1973; Elias *et al.* 1981; Graham *et al.* 1987), has more recently been attributed to a lack of emission lines in that region (Spyromilio, Pinto & Eastman 1994; Meikle *et al.* 1997).

In this paper we present near-IR spectra of seven Type Ia supernovae, namely SNe 1986G, 1991T, 1992G, 1994ae, 1995D, 1995al and 1996X. The 92G, 94ae, 95al and 96X spectra are presented for the first time. These observations span epochs 13 days to 338 days, thus providing the most extensive temporal coverage ever achieved for Type Ia SNe NIR spectra. While this work focuses on those spectra taken during the nebular phase only, for completeness we have also included several spectra taken during the earlier photospheric phases of some of these supernovae. Type Ia NIR spectra in the photospheric phase have already been presented and discussed by Frogel *et al.* (1987), Lynch *et al.* (1990, 1992) and Meikle *et al.* (1996, 1997). For the nebular phase spectra, line identification and interpretation is carried out using our non-LTE, nebular spectral synthesis code. We shall use this analysis to (a) identify the lines (b) investigate the origin of the J-band deficit, (c) determine the evolution of the cobalt/iron mass ratio, and (d) estimate the absolute mass of ^{56}Ni ejected.

2 Observations

Descriptions of the seven Type Ia supernovae under consideration are given in Table 1. Infrared spectra, taken at ten epochs spanning 13 to 338 days post-maximum blue light are shown in Figures 1 & 2. The observing log for the NIR spectra is in Table 2. The SN 1986G spectra were acquired with CGS2 at UKIRT, while the day 60 spectrum of SN 1991T was obtained with IRIS at the Anglo-Australian Telescope (AAT). All the other infrared spectra were acquired using the cooled grating spectrograph, CGS4, at the United Kingdom Infrared Telescope (UKIRT) with the short focal length (150 mm) camera and either the 75 or 150 l/mm grating. Sky subtraction was achieved by nodding between two positions along the slit. Data reduction was carried out using the CGS4DR (Daly 1996) and Figaro (Shortridge 1995) packages. Except where stated otherwise, the CGS4 wavelength calibration was with respect to krypton and argon arc lamps. Where roughly contemporary optical spectra are available, these are shown in Fig. 3. The observing log for the optical spectra is given in Table 3.

Since our aim was to simultaneously model contemporary NIR *and* optical spectra, close attention was given to both relative and absolute fluxing. Only for SN 1995D was there a sufficiently high signal-to-noise overlap in the optical and NIR spectra (0.85–1.04 μm) to allow the relative fluxing to be directly checked. It was found that the total flux in the overlap range as measured from the NIR and optical spectra differed by only 1%. This suggests not only that the relative fluxing was good but also, given that the NIR and optical data were obtained at different times, at different sites and with different instruments, it gives us confidence about the quality of our absolute fluxing.

All spectra were absolute flux-calibrated using flux standards. In addition, the fluxing was checked by comparing our observed spectral fluxes in the standard pass-bands with those derived by extrapolation from photometry, using Type Ia light curves. Fluxing in the optical band was checked by extrapolating early-epoch V-band photometry to the epochs of our observations, using the standard V-band light curve of Doggett & Branch (1985). These magnitudes were then compared with our observed total spectral flux in a square passband spanning 0.5055–0.5945 μm . For SN 1995D at 92 d and 1995al at 176 d the broadband flux obtained by extrapolation exceeded the observed total spectral flux by about 30%. For SN 1991T, the difference was less than 5%.

Absolute fluxing in the NIR band was checked as follows. Using IRCAM2 at UKIRT, H- and K-band photometry of SN 1995al was obtained at 162 d. No NIR light curves are available for this era and so we used the I-band light curve of Schlegel (1995) to extrapolate to 94 d and 175 d. The extrapolated fluxes were then compared with the total observed spectral fluxes in square passbands spanning 1.45–1.85 μm and 1.9–2.5 μm . We found that the spectral fluxes tended to exceed the extrapolated broadband fluxes by about 15 %. For SN 1994ae at 174 d we followed a similar procedure, extrapolating from AAT/IRIS H-photometry obtained at 120 days (courtesy of J. Spyromilio). In this case, the spectral flux was fainter than the extrapolated value by $\sim 40\%$, but the signal-to-noise is very low. For SN 1995D, no NIR photometry was available. We therefore scaled the observed NIR spectral flux by an amount equal to the difference

in the peak V-magnitudes of SNe 1995D and 1995al. This was then compared with the extrapolated H-band flux as for SN 1995al. We found the observed spectral flux was less than the extrapolated broadband value by 15%. Only for the NIR fluxing of SN 1991T at 338 d was a photometry check not possible due to the non-availability of reliable infrared light curves extending to such a late epoch.

Given that the square passbands we adopted only roughly approximate the shape of the photometry passbands used, we conclude that the agreement between the measured spectral fluxes and the extrapolated values is encouraging. It seems unlikely that the fluxing of either the optical or NIR spectra was in error by more than $\sim 25\%$. Such an error is small compared with other modelling uncertainties discussed later.

2.1 SN 1986G

SN 1986G occurred in the dust lane of NGC 5128 (Cen A). Its B–V colour (Hill 1986; Phillips and Geisler 1986), ultraviolet spectra (Wamsteker *et al.* 1986; Kirshner 1986) and Na I D and Ca II H,K absorption lines observed at the redshift of the parent galaxy (Tonry and Strauss 1986; Heathcote, Cowley and Hutchings 1986) all indicate that the supernova was substantially reddened. In addition infrared light curves showed that SN 1986G was intrinsically atypical (Frogel *et al.* 1987). Spectra spanning $\sim 1\text{--}2.5\ \mu\text{m}$ for the period 13 to 30 days were acquired by Frogel *et al.* (1987) and Graham *et al.* (1987) (spectra published in Meikle *et al.* 1997). These were the first-ever NIR spectra of a Type Ia event. The two spectra of Graham *et al.* are included in Fig 1.

2.2 SN 1991T

The photospheric-phase behaviour of SN 1991T was atypical. At peak it was exceptionally luminous. It also exhibited strong iron-group lines in its pre-maximum spectra, plus weaker-than-normal intermediate-mass spectral features. NIR spectra of SN 1991T and their analysis have been presented in Meikle *et al.* (1996) (day ~ 0), Spyromilio *et al.* (1994) (day 60), and Spyromilio *et al.* (1992) (day 338). The days 60 and 338 spectra are included in Figs. 1 & 2 respectively. An optical spectrum at about the same phase as the day 60 NIR spectrum was obtained in AAT service time and is shown in Fig. 3. Also shown is an AAT service spectrum taken on day 403.

2.3 SN 1992G

The NIR spectrum of SN 1992G was obtained using the 75 line mm^{-1} grating and 58×62 pixel array at three wavelength settings to cover the wavelength range 1.0–1.8 μm . A one pixel (3 arcsec) wide slit was used, oriented at a position angle of 21° . The J-band was covered on day 39, and the H-band on day 40. Atmospheric

OH lines were used to calibrate the wavelength scale. The flux standard was BS4078. No contemporary optical spectra were available. However, in Fig. 3 we show a 17 day spectrum taken by R. Lopez and G. Gomez using the Faint Object Spectrograph (FOS) on the Isaac Newton Telescope (INT). We obtained the spectrum from the La Palma Data Archive in unreduced form. We reduced the spectrum using the Figaro data reduction package (Shortridge 1995). CuAr or CuNe arc lamp spectra were used for wavelength calibration, and the spectrophotometric standard star, G138-31, provided flux calibration. The spectral coverage and resolution is given in Table 3. The optical spectrum suggests that SN 1992G was, spectroscopically at least, a normal Type Ia supernova.

2.4 SN 1994ae

The day 175 NIR spectrum of SN 1994ae was acquired with the very recently upgraded CGS4 with a 256×256 InSb array and the 75 line mm^{-1} grating, under ‘shared risks’ conditions. Owing to a technical problem, we had to use a 1.25 arcsec (1 pixel) wide slit, which meant that the absolute fluxing was less reliable than usual. The slit was placed east-west to minimize the gradient of galaxy background light. The flux standard was HD 84800. The NIR spectrum is shown in Fig. 2. We also obtained an optical spectrum of SN 1994ae at 89 days using ISIS on the William Herschel Telescope (WHT). The flux standard was Feige 34. The optical spectrum is shown in Fig. 3 and is typical of a Type Ia supernova at this phase. Unfortunately we were unable to acquire an optical spectrum more closely contemporary with the IR observation.

2.5 SN 1995D

The day 92 NIR spectrum of SN 1995D was obtained with the same instrument configuration as for SN1994ae. The data were reduced in the usual way (see above) using HD 77281 as the flux standard. A contemporary optical spectrum is shown in Fig 3. This spectrum is courtesy of A. Filippenko and D. Leonard and was taken on day +96 with the Lick Observatory Shane 3 m telescope using the cooled germanium spectrograph. The spectrum, which covers the 0.36 to 1.02 μm range, is typical of a Type Ia at this phase, showing an abundance of singly- and doubly-ionized Co and Fe emission lines.

2.6 SN 1995al

IR spectra were obtained at 94 and 176 days. For the day 94 spectrum the 75 line mm^{-1} grating was used. In view of the good seeing that night, a 1-pixel-wide slit (1.25 arcsec) was selected, oriented east-west. The flux standard was HD 84800. Some difficulty in subtracting off the galaxy background was experienced owing to the steep

and rapidly changing gradient in the supernova vicinity. For the day 176 spectrum we used the 150 line mm^{-1} grating and a 2-pixel-wide slit (2.5 arcsec) oriented 63° north-west to minimize the gradient of galaxy light along the slit. The flux standard used was HD 84800. We encountered a problem in the reduction of the 3rd-order J-band 0.985–1.30 μm spectrum, owing to inadequate blocking of 2nd-order H-band emission. In order to remove this 2nd-order contamination the observed H-band spectrum was divided by the function for the blocking filter used in the H-band and multiplied by the blocking filter function for the J-band. The wavelength of the resulting spectrum was then multiplied by 2/3 to produce an estimate of the J-band contamination spectrum. This was then used to decontaminate the supernova and standard spectra. The supernova spectrum was flux calibrated as normal using the decontaminated standard star spectrum. An optical spectrum (Fig. 3) was obtained at 149 days through INT service using the Intermediate Dispersion Spectrograph (IDS) and the R150V grating. As for the 176 day NIR observation, the slit was oriented at 69° to minimize the galaxy gradient. Feige 19 was the flux standard. The optical spectrum is typical of a Type Ia event at this phase.

2.7 SN 1996X

The day 19 NIR spectrum was acquired using the same CGS4 settings as for the day 176 SN 1995al spectrum. BS4935 was used as the flux standard.

2.8 Summary of the infrared spectra

All nine of the NIR spectra in the 13 to 176 day era extend to wavelengths as short as 1.1 μm and usually to 1.0 μm (Figs. 1 & 2). They *all* show a characteristically dramatic decline in the ~ 1.02 – 1.13 μm region. In addition, spectra taken on or after day 40 usually exhibit a relatively isolated feature at ~ 1.26 μm . All seven spectra taken between 13 and 94 days show a sharp rise at ~ 1.50 μm . Thus, we confirm that the well-known red J-H colour results from a flux deficit between 1.13 and 1.50 μm and our spectra demonstrate that this deficit is responsible for the red colour to at least 94 days. Two of the spectra (91T at 60 d, 95D at 92 d) span the 0.9 to 1.0 μm region. These reveal a strong, multi-peaked feature. In the range 1.5–1.8 μm , SN 1991T exhibits a relatively featureless band of emission on day 60, replaced by day 338 by a prominent single peak at 1.65 μm . Both SN 1995D and SN 1995al at ~ 90 days show a distinct emission feature at 1.56 μm , with more complex blends in the 1.67–1.80 μm region. In the 2–2.4 μm range between day 13 and 92 the spectra exhibit a very characteristic, and remarkably unchanging multi-peaked structure.

3 Spectral Model

In order to identify and interpret the observed IR features, we have constructed a non-LTE nebular spectral model and applied it to all of the spectra at epochs later than 90 days. For this initial investigation we confined the model to lines of cobalt, iron and sulphur. In the case of a thermonuclear scenario, cobalt and iron are expected to dominate the NIR and optical spectra. Strong lines of singly- and doubly-ionized sulphur are also expected to contribute to the multi-peaked structure in the J-band. However, a complete description should also include other lighter elements such as silicon and magnesium.

Several simplifying assumptions are made. The electron temperature and ionization state of the gas are constant throughout the nebula. In addition, the total line fluxes, including the effects of line-trapping (see below) are calculated assuming a constant density. Consequently the profiles of optically-thin lines are parabolic. In general, a relatively weak continuum, probably due to blends of many weak lines, was also present in the observed spectra. This was represented with a flat continuum in the model. Since cobalt and iron have similar ionization potentials in the singly- and doubly-ionized states, we set N_{Co^+}/N_{Fe^+} and $N_{Co^{2+}}/N_{Fe^{2+}}$ to be equal to the total cobalt/iron abundance ratio. The cobalt lines are due to radioactive ^{56}Co (the decay product of ^{56}Ni) and the iron lines come from both ^{56}Fe (the stable decay product of ^{56}Co) and also from other stable iron isotopes formed before and during the explosion. For these other iron isotopes, the mass is 19% relative to the total iron mass (Nomoto, Thielemann, and Yokoi 1984).

The $^{56}Ni \rightarrow ^{56}Co \rightarrow ^{56}Fe$ light curve hypothesis implies that we should expect the nebular-phase spectra to be dominated by singly- and doubly-ionized lines of Fe and Co. We therefore included model atoms (number of levels in brackets) for Fe^+ (44), Fe^{2+} (27), Co^+ (25) and Co^{2+} (17). A 25-level Fe^o atom was also included since the red wing of one of its strongest lines, [Fe I] 1.443 μm , was covered by some of our data thus providing the possibility of constraining the abundance of this species. We did not include a Co^o atom as no strong [Co I] lines occur in our optical-NIR spectral range. Transitions of [Fe IV] and [Co IV] do occur in our spectral range, but they arise from energy levels with excitation potentials higher than 32000 cm^{-1} and 23000 cm^{-1} respectively and so are expected to be weak. Strong [S II] and [S III] lines exist in the 0.95 and 1.02 μm region and so 5-level atoms of S^+ and S^{2+} were also included. However, since the major aim of this paper is to test the ^{56}Ni hypothesis, we have not included any other intermediate-mass element transitions in either the NIR or optical regions.

During the supernova era covered by this work, for many of the lines the density is expected to fall below the critical value. Hence a non-LTE treatment is necessary i.e. we assume that the levels are populated by the combined effects of electron collisions in an isothermal gas and spontaneous decay. We include the effects of line trapping in an expanding atmosphere i.e. the downward radiative rates are modified by the Sobolev escape probability (Sobolev 1960). The detailed balance equations between thermal

electron collisions and spontaneous decays are solved by matrix inversion. We have not treated the non-thermal excitation/de-excitation and ionization/recombination driven by the gamma-rays, high energy electrons and positrons.

For [Fe I], transition probabilities are taken from Fuhr, Martin & Wiese (1988), and the collision strengths from Pelan & Berrington (1996). For [Fe II], transition probabilities are from Nussbaumer and Storey (1988b) & Fuhr *et al.* (1988), and collision strengths from Pradhan & Zhang (1993 & 1995). For [Fe III], transition probabilities are from Nahar & Pradhan (1996) and collision strengths from Zhang & Pradhan (1995) and Zhang (1996). For [Co II], the transition probabilities are from Nussbaumer & Storey (1988a) and a compilation of Kurucz (1988). For [Co III], transition probabilities are from Fuhr *et al.* (1988), Hansen (1984) and from a compilation of Kurucz (1988). For [S II], transition probabilities are from Mendoza & Zappa (1982), and the collision strengths from Cai & Pradhan (1993) and the 1983 Mendoza compilation. For [S III], transition probabilities and collision strengths are from the 1983 Mendoza compilation and the Kurucz list (1975). A major uncertainty in this work is caused by the inaccurate A-values for doubly-ionized cobalt and the lack of collision strengths for singly- and doubly-ionized cobalt. Only for the a^2G-a^4F transitions are collision strengths available (Kurucz 1988). All the other collision strengths for [Co II] and [Co III] were determined using the approximation

$$\Omega_{ij} = \omega g_i g_j$$

where $\omega=0.02$ (Axelrod 1980; Graham, Wright & Longmore 1987). This has been found to yield collision strengths with errors of up to about a factor of two relative to precise calculations.

The models were reddened by the appropriate amount. For each case, the extinction was obtained by two methods. In the first method, the supernova (B-V) colours were compared with the zero-extinction colour template of Phillips *et al.* (1992) or Doggett & Branch (1985). In the second method, E(B-V) was found from the equivalent width (EW) of the interstellar Na I D absorption line, and applying the relation $EW=4 * E(B-V)$ (Barbon *et al.* 1990). It was found that these two methods produced values which usually agreed to within 20%. Assuming $E(B-V)=3.1A(V)$, the full spectral reddening function for each supernova was then obtained from the empirical extinction law of Cardelli *et al.* (1989).

Estimation of the distances to the supernovae was a problem. An obvious method is to use the light curves of the actual supernovae (*cf* Reiss *et al.* 1995). However, a light curve was available for *only* SN 1991T. We therefore estimated the distances of the parent galaxies using the Aaronson *et al.* (1982) infall model (rms dispersion of 150kms^{-1}), taking the distance of the Virgo Cluster to be 16 ± 1.5 Mpc (Van Den Bergh 1996). We note that for SN 1991T, this procedure gave a distance of 14.4 Mpc, in reasonable agreement with the light curve-based 12 Mpc quoted by Reiss *et al.* (1995), and the 16.2 ± 2 Mpc of Höflich (1995). The adopted distances are given in Table 4.

While distance is clearly a critical parameter in absolute mass estimation it can, to a lesser extent, also influence the determination of the cobalt/iron mass ratio. As

explained below, a critical step in the determination of the mass ratios is the matching of model line flux *ratios* to those observed. For the cases where the lines involved are optically thin and where the electron density is above the critical density, the line flux ratios are independent of distance. However, in situations of non-negligible optical depth or below critical density, the density can influence the line ratios. To match the flux in a particular line requires the population density, supernova radius and distance. The supernova radius is obtained from the observed expansion velocity and time since explosion. For a given spectrum, a change in distance requires a density change to maintain the match to the data. However, the effects of optical depth and critical density mean that the required change in density for a given distance change may be different for different transitions. Thus even when determining mass ratios it can be necessary to have an independent estimate of the distance although, as already indicated, the dependence of a given line *ratio* on distance/density is usually weak.

Initially we set the Co/Fe mass ratio at the value expected assuming all the cobalt and iron results from ^{56}Ni decay. Electron temperature and ion densities were then adjusted to reproduce the ratios of particular, prominent lines. (The total electron density was set by the ion densities). In addition to iron-group lines, [S II]1.03 and [S III]0.953 μm were included. Adopting the same temperature as for the iron-group spectra, the abundance of S^+ and S^{2+} was adjusted to match the strong features in the 0.9–1.1 μm region. To test the radioactive decay hypothesis, the Co/Fe mass ratio was then varied and the temperature and densities were adjusted where possible to provide a reasonable match to the spectra. In this way we found the range of mass ratios which would provide a plausible fit to the data. Using the model fits, for each species we also determined the absolute mass assuming a radius given by the product of the expansion velocity and the age of the supernova.

4 Results

All the spectra with their best visually-matched models are shown in Figs. 4–12 and the model parameters are listed in Tables 4 and 5. Tables 6, 7 and 8 give the peak wavelengths of the main features present in each spectrum together with the identity and flux of the main contributing transitions derived from the models. It can be seen that there is a wealth of doubly- and singly-ionized iron and cobalt lines in both the optical and infrared regions. In both the NIR and optical regions, for relatively isolated features of good S/N, the line widths were reasonably reproduced with expansion velocities in the range of 8– 8.5×10^3 km/s.

4.1 Individual Supernovae

For SN 1995D at 92 d (Figs. 4, 5 & 6) the model electron temperature and Co^{2+} density were adjusted to provide the best visual match to the [Co III]0.589/0.591 μm /

[Co III]2.002 μm line flux ratio. (As noted above, the $a^4\text{F}-a^2\text{G}$ [Co III]0.589/0.591 μm transitions are two of the few cobalt transitions for which collision strengths *are* available.) The ionization ratio for cobalt was then determined by adjusting the relative abundance of Co^+ to match the 1.55 μm feature which is a blend dominated by [Co II]1.547 μm and [Co III]1.549 μm . The iron spectra were then formed by using the same electron temperature, assuming the ^{56}Ni cobalt/iron mass ratio and adopting the same ionization ratio as for cobalt. In the NIR spectrum (Figs. 5 & 6), it can be seen that in addition to the 1.55 and 2.002 μm features, emission at 1.76, 2.15 and 2.24 μm are reproduced by [Co III] and [Fe III] transitions although the model flux is somewhat weak here. However, emission in other parts of the NIR spectrum remain unexplained. These include regions around 1.00, 1.10, 1.27 and 1.65 μm . While the emission at 1.27 μm is almost certainly due to a blend of [Co III] and [Fe II] lines, adjusting the temperature or ionisation ratio to force a match here results in severe overproduction of either [Co III]0.589/0.591 μm or [Fe II]0.44 μm .

For the optical spectrum (Fig. 4) the model is less successful. Many of the discrepancies in this region may well be due to the inaccurate A-values for doubly-ionised cobalt and for the [Fe II] $a^2\text{G}$ term. Another probable cause is the non-inclusion of intermediate-mass elements in the model such as silicon and magnesium. A third possibility is suggested by a preliminary calculation using a more complete model, which shows that the ion fraction of $\text{Fe}^{2+}/\text{Fe}^+$ increases with radius. The total flux which results is the average over this distribution and may not be achievable from any single ionization ratio. A curious discrepancy is that emission in the 0.43-0.44 μm region is underproduced by the model, with the shortfall worsening with time. A similar effect can be seen in the model fits of Ruiz-Lapuente (1992) for SN 1986G at 257, 296 and 323 days. Using a more sophisticated model, Liu, Jeffery & Schultz (1997) also find this effect, although in their study it only becomes a problem at about 1 year. They suggest that by these late times a significant contribution to the Fe II emission may come from the recombination or charge transfer cascades from Fe^{2+} . They also suggest time-dependent effects or emission from other species as alternative explanations. Another interesting result from the model comparison is that strong observed features at 0.47 μm and 0.589/0.591 μm are blueshifted with respect to the model [Fe III] 0.47 μm and [Co III] 0.589/0.591 μm lines by ~ 3500 km/s and ~ 1500 km/s respectively. Blueshifts of ~ 1000 km/s are also apparent for the features at 1.56 and 2.01 μm . We note that the 89 d optical spectrum of SN 1994ae exhibits similar blueshifts to those seen in SN 1995D.

For SN 1995al at 94 d (Fig. 7) only an infrared spectrum was available. In this case we were unable to pin down the electron temperature, ion density or ionization ratio. Therefore we assumed the same electron temperature as for SN 1995D at a similar epoch. The $\text{Co}^+ + \text{Co}^{2+}$ densities *and* the ionization ratios were adjusted to provide a match to the observed $([\text{Co II}]1.547 + [\text{Co III}]1.549 \mu\text{m}) / [\text{Co III}]2.002 \mu\text{m}$ flux ratios. As with SN 1995D at 92 d, the 1.76 μm feature is partially reproduced by a blend of [Co II] and [Co III] lines. Unfortunately the 2.15 and 2.24 μm features were not covered by the observations. Again, similarly to SN 1995D at 92 d, observed emission around 1.10 and 1.65 μm is unaccounted for. However, the match to the feature at 1.27 μm is more satisfactory. The blueshifts seen in the NIR spectra of SN 1995D are not apparent

in the SN 1995al data.

For SN 1995al at +176d (Figs. 8 & 9), the relatively low S/N and the smaller wavelength coverage in the NIR (Fig. 9) prompted us to use only the 149 day optical spectrum (Fig. 8), scaled to roughly match the epoch of the infrared spectrum, for determining the model parameters. The temperature was adjusted to provide a match to the observed $[\text{Co III}]0.589/0.591 \mu\text{m}/[\text{Fe III}]0.466/0.470 \mu\text{m}$ flux ratio. The ionization ratio was then adjusted to match the $[\text{Fe II}]0.716/0.717 \mu\text{m}$ flux. The resulting NIR spectrum was then compared with the data. Given the low S/N in the NIR, the model is reasonably consistent with the observed NIR spectrum of SN 1995al. Nevertheless, there is still unexplained emission around $1.26 \mu\text{m}$ and $1.65 \mu\text{m}$. In the optical region, even allowing for the additional deliberate model match in the $0.716 \mu\text{m}$ region, the match is significantly better than for the $\sim 90\text{d}$ spectra. In particular, the wavelength agreement of the strong $0.47 \mu\text{m}$ and $0.59 \mu\text{m}$ features with the model is much better than for SN 1995D at 92 d. There is no evidence of a blueshift in the $0.59 \mu\text{m}$ feature, while at $0.47 \mu\text{m}$ the shift is less than $\sim 1000 \text{ km/s}$. Unfortunately we do not have an earlier optical spectrum for SN 1995al to compare with the $\sim 90 \text{ d}$ SN 1995D and SN 1994ae spectra.

For SN 1994ae at 175 d (Fig. 10) only an infrared spectrum was available. Therefore a similar approach was adopted as for SN 1995al at 94d, using the same electron temperature as for SN 1995al at 176 d. The greater uncertainty in the model parameters due to the lack of an optical spectrum, was worsened by the very low S/N of the NIR spectrum, even after binning by a factor of four. The model appears to account for the emission at 1.03 , 1.55 and $1.65 \mu\text{m}$ but there is unexplained emission around 1.10 , 1.22 and, possibly, $1.75 \mu\text{m}$.

For SN 1991T a contemporary optical spectrum was derived by approximately scaling the day 403 optical spectrum to the epoch of the day 338 NIR spectrum (Figs. 11 & 12) (see Spyromilio *et al.* 1992). The model electron temperature was adjusted to provide a match to the observed $[\text{Fe II}]0.717 \mu\text{m}/[\text{Fe II}]1.644 \mu\text{m}$ flux ratio. The ionization ratio was adjusted to match the $[\text{Fe III}]0.466/0.470 \mu\text{m}$ flux. The cobalt spectra were then formed by using the same model parameters, assuming the radioactive scenario mass-ratio. The resulting IR/optical model, dominated by iron line emission, is gratifyingly similar to the observed spectra. Even the K-band emission seems to be reproduced by $[\text{Fe III}]$ lines, although the S/N is low. As suggested by Ruiz-Lapuente (1992), much of the unreproduced emission in the $0.7\text{--}0.95 \mu\text{m}$ region may be due to (stable) ^{58}Ni , via the transitions $[\text{Ni II}] 0.7380 \mu\text{m}$ and $[\text{Ni III}] 0.7899 \mu\text{m}$. In agreement with Spyromilio *et al.* (1992), we conclude that the success of the model fit here supports the prediction of the ^{56}Ni scenario that over 96% of the original nickel should have decayed to iron by this epoch. We believe that the remaining $\sim 4\%$ of cobalt is still apparent in the $[\text{Co III}] 0.589/0.591 \mu\text{m}$ feature.

4.2 Consistency Checks

Following Spyromilio *et al.* (1992), we applied two simple consistency checks to the individual models. Firstly, for each supernova we made an independent estimate of the atomic density by distributing $1 M_{\odot}$ of iron-group elements throughout a sphere defined by the maximum velocity and epoch. We found that the atomic densities derived in this way agreed to within a factor of three of the total densities obtained from the spectral models.

Secondly, the heating and cooling rates of the gas were compared. Energy is deposited in the ejecta by the decay of ^{56}Co at a rate of

$$5.80 \times 10^{-13} e^{-t/113} (f + 0.035) \text{ ergs}^{-1} \text{ atom}^{-1}$$

where t is the time in days after the explosion and f is the fraction of γ -rays absorbed (Axelrod 1980). f varies as t^{-2} so that we would expect f -values of ≥ 0.5 at 3 months and ~ 0.1 at 6 months to a year for the supernovae studied. We compared predicted heating rates with the three cases for which we have both optical and NIR spectra. We find that the observed total optical+NIR luminosities correspond to cooling rates about a factor of two below the heating rates. Given that, in each case, only part of the total supernova spectrum was used we conclude that the predicted heating rates were in reasonable agreement with the cooling rates.

4.3 Discussion of the model matches

We find that a spectral model based on ^{56}Co -decay can be adjusted to reproduce several of the prominent features in the NIR and optical spectra of Type Ia supernovae at three distinctly different epochs (3, 6 and 11 months). At 3 and 6 months, feature identifications include [Co III]0.589, 0.591 μm , [Co III]2.002 μm , [Co II]1.547 μm –[Co III]1.549 μm , [Fe III]0.466, 0.470 μm , while at 11 months [Fe II]0.717, [Fe II]1.257 and [Fe II]1.644 μm are prominent. Plausible temperatures and densities are also found (cf. Axelrod 1980). There does exist some unexplained emission in the J- and H-windows in the 3–6 month period. However, the fact that this does not occur at 1 year indicates that the problem may lie with the modelling of the cobalt lines which contribute significantly at the earlier epochs. We suspect that inaccuracies in the atomic data for cobalt may be at least part of the problem.

As pointed out earlier, there is a possibility that Na I D contributes to the 0.59 μm feature. Since our wavelength coverage extends into the NIR we are able to use Na I 2.21 μm to estimate the strength of Na I D. For LTE conditions at a temperature of ~ 7000 K we would expect Na I 2.21 μm to have a flux level of $\sim 3\%$ of Na I D. For SN 1995D, the flux around 2.2 μm has a flux of about 1% that of the 0.59 μm feature. While this does not rule out the presence of Na I D in the 0.59 μm feature, it does seem

unlikely that it could be the dominant contributor. We also note that in our model fitting we found no need for the addition of sodium to improve the match.

While encouraging, these results alone do not rule out the possibility that a similar success could be achieved with a completely different model having the requisite number of freely-adjustable parameters. However, having adjusted our model to match the above specific features, we find that a number of other spectral lines are also successfully explained, particularly in the NIR. These are [Co III]1.742/1.764 μm , [Fe III]2.146 μm and [Fe III]2.243 μm . The ability of our model to *predict* these other features gives us added confidence in the appropriateness of the ^{56}Co -decay hypothesis.

In spite of the relative success of the ^{56}Ni -based model in reproducing much of the observed NIR and optical nebular spectra, it is important to check the range of cobalt-to-iron mass ratios which uncertainties in the observed spectra, atomic data and distances would allow. At our earliest phase (~ 3 months), the electron density is above the critical value (i.e. the electrons are in LTE) and yet the lines have become optically thin. Consequently, as explained above, derived mass ratios are distance independent. However, A-value uncertainty is still important. The mass ratio for a particular degree of ionization under LTE conditions can be expressed analytically as:

$$\frac{M_{\text{Co}_n}}{M_{\text{Fe}_n}} = \frac{I_{ji}}{I_{j'i'}} \times \frac{\lambda_{ji}}{\lambda_{j'i'}} \times \frac{A_{j'i'}}{A_{ji}} \times \frac{g_{j'}}{g_j} \times \frac{e^{-E_{j'}/kT}}{e^{-E_j/kT}} \times \frac{Z_{\text{Co}_n}}{Z_{\text{Fe}_n}} \times \frac{m_{\text{Co}}}{m_{\text{Fe}}}$$

where Co_n and Fe_n indicate ions of the same degrees of ionization, I is the line flux, λ the transition wavelength, A the Einstein A-value, g the statistical weight, E the upper level energy, Z the partition function, m the atomic mass and the subscripts ji and $j'i'$ represent the transitions in the relevant cobalt and iron ion lines respectively. At later epochs the spectrum is produced under increasingly non-LTE conditions. In general, this means that the derived mass ratio is sensitive to uncertainties in both A-values and collision strengths, as well as (to a lesser extent) distance, as explained above. In this regime, we do not have a simple analytical expression for the mass ratios. For both LTE and non-LTE conditions, to determine the effects of our imprecise knowledge of the atomic data we assumed Gaussian distributions in their uncertainties and used a Monte Carlo simulation to find the range of mass ratios for which a match to the observed spectra was still obtainable. A change in temperature will also produce a change in the mass ratio. The effect is strongest in the Boltzmann factor, producing around $\pm 10\%$ in the mass ratio for $\Delta T = \pm 500\text{K}$, which is the typical temperature range that the model fits permit. The partition functions are also sensitive to temperature, but their *ratios* are much less sensitive, typically remaining within $\pm 5\%$ for $\Delta T = \pm 1000\text{K}$. In addition, distance uncertainty can have a small influence on the mass ratio for non-LTE conditions. Taking these various effects into account, we find that the values of $M_{\text{Co}}/M_{\text{Fe}}$ are uncertain by factors of ~ 1.5 to ~ 4 depending on the availability and quality of the data. These ranges are shown in Table 9.

5 Absolute mass estimates

We also used the model fits to estimate the *absolute* masses of ^{56}Ni produced in each supernova. In Table 10 we present the masses of the individual species, together with the total mass of ^{56}Ni obtained by summing the singly- and doubly-ionized iron and cobalt. We include upper limits for neutral iron and cobalt. The neutral iron limit was estimated from the region of the H-band which covers part of the [Fe I]1.443 μm feature. The neutral cobalt limit was then derived assuming the same ionization fraction and the radioactive decay mass ratio. We find that the contribution of neutral cobalt and iron to the total iron-group mass is generally less than 15%. In the case of SN 1995al at +176 days the H-band spectrum does not extend far enough blueward to allow us to place an upper limit on neutral iron and cobalt. Unfortunately, triply-ionized cobalt or iron do not produce any prominent emission lines in the NIR or optical region and so a significant mass of either cannot be ruled out by the data. Axelrod (1980) estimates that the contribution of triply-ionized material could be about 10% of the total mass at 3 months rising to $\sim 25\%$ at 6 months and $\sim 40\%$ at one year. These estimates are therefore also included in Table 10. However, the values for the total ^{56}Ni mass shown in Table 10 are conservative as they are obtained by summing the singly- and doubly-ionized iron and cobalt only.

As with the mass ratio study, absolute mass determination is subject to atomic data uncertainty. In general, however, it is more sensitive to temperature, distance and extinction uncertainty. The effect of all these uncertainties is that the derived masses are uncertain by factors of ~ 1.5 to ~ 4 , again depending on the availability and quality of the data (see Table 10). We note that the level of uncertainty in the mass *ratio* estimates is not significantly less than this, in spite of their lower sensitivity to distance and temperature errors. This is because the atomic data uncertainties, dominate the overall error for both the relative and absolute masses.

For SNe 1991T, 1995D and 1995al our estimates for the total ^{56}Ni mass of all four ionization states are in the range 0.37–0.90 M_{\odot} . If we confine our mass estimate to the directly measured singly- and doubly-ionized species only, the mass is 0.27–0.67 M_{\odot} . The total ^{56}Ni mass for SN 1994ae is found to be only about 0.2 M_{\odot} but it must be remembered that the data in this case are of very low signal-to-noise. and at least twice this amount is possible. Thus, in spite of the uncertainties, the values found point towards the ejection of substantial masses of ^{56}Ni , and so support the basic thermonuclear scenario.

6 Summary and Conclusions

In this paper we have presented the most extensive NIR spectral coverage hitherto of Type Ia supernovae, spanning 13 to 338 days after maximum blue light. In some cases, contemporary or near-contemporary optical spectra were also shown. The NIR spectra

are highly structured throughout the J-, H- and K-bands. In particular, all nine spectra in the 13 to 176 day era show a characteristically steep decline in the $\sim 1.02\text{--}1.13\ \mu\text{m}$ region, while all seven spectra taken between 13 and 94 days show a sharp rise at $\sim 1.50\ \mu\text{m}$. We conclude that the $1.13\text{--}1.50\ \mu\text{m}$ deficit is responsible for the red colour for the entire period from 13 to at least 94 days.

Comparison of the nebular-phase spectra with a simple non-LTE spectral model based on ^{56}Ni -decay abundances, indicates that significant fractions of both the NIR and optical spectra are made up of iron and cobalt lines. Singly-ionized sulphur also contributes strongly to the emission around $1\ \mu\text{m}$. We conclude that the $1.13\text{--}1.50\ \mu\text{m}$ deficit is due to a lack of emission lines from species which dominate the rest of the IR/optical spectrum, as originally proposed by Spyromilio, Pinto and Eastman (1994). Identified NIR features include $[\text{Fe II}]1.257\ \mu\text{m}$, $[\text{Fe I}]1.443\ \mu\text{m}$, $[\text{Co II}]1.547\ \mu\text{m}$ – $[\text{Co III}]1.549\ \mu\text{m}$, $[\text{Fe II}]1.644\ \mu\text{m}$, $[\text{Co III}]1.742\text{--}1.764\ \mu\text{m}$, $[\text{Co III}]2.002\ \mu\text{m}$, $[\text{Fe III}]2.146\ \mu\text{m}$ and $[\text{Fe III}]2.243\ \mu\text{m}$. Failure to account for some of the NIR emission in the 3–6 month period may be partly due to inadequate atomic data for cobalt.

The model comparison for SN 1995D at 92 d revealed blueshifts in the features at $0.47\ \mu\text{m}$, $0.589/0.591\ \mu\text{m}$, $1.56\ \mu\text{m}$ and $2.01\ \mu\text{m}$. Similar shifts were seen in the optical spectrum of SN 1994ae at 89 d. However, for the 94 d NIR spectrum and 149 d optical spectrum of SN 1995al, the blueshifts were much smaller or non-existent. At later epochs the blueshifts diminished or disappeared altogether. The fact that the SN 1995D blueshifts occurred at several places over the entire NIR-optical spectrum tends to argue against blending with unidentified lines as the general cause, although this may be a partial explanation for the larger blueshift at $0.47\ \mu\text{m}$. In addition, all the model lines are optically thin and so the effect cannot be simply one of optical depth in a homogeneous medium. We therefore suggest the ejecta are actually inhomogeneous and that the blueshifts are due to density enhancements which are optically thick. Some support for this is provided by the fact that small or no blueshifts were seen at 6 and 11 months.

Our ^{56}Ni -based model, using plausible temperatures and densities, both accounts for and predicts features in the NIR and optical regions. In particular it shows that the cobalt lines decay with time relative to the iron lines and that this is due to the decline in the abundance of cobalt at the ^{56}Co -decay rate. This gives us confidence in the appropriateness of the ^{56}Ni -decay light-curve hypothesis. Nevertheless, there are important discrepancies between the model predictions and the observations. This is probably due to a combination of unidentified lines, inaccurate atomic data, and the use of a simple spectral model. In spite of the large uncertainties in various parameters, *we nevertheless conclude that the mass of ejected ^{56}Ni is large*. We believe that, on balance, our results support the basic thermonuclear explosion scenario and argue against the core-collapse model of Colgate *et al.* (1997), at least for most Type Ia supernovae. The range of values encompasses predictions of white-dwarf-merger, delayed-detonation and sub-Chandrasekhar mass models.

The work presented here is only a first attempt to describe and interpret the late-time

NIR behaviour of Type Ia supernovae. Compared with the optical band, the quantity and quality of spectra are still much inferior. However, the introduction of more sensitive NIR detectors coupled with adaptive optics means that rapid improvement in data quality can be anticipated in the near future. Indeed it may become possible to detect the presence of other radioactive isotopes such as ^{57}Co (*cf* Varani et al. 1990). The development and application of more self-consistent and comprehensive spectral synthesis codes such as EDDINGTON (Eastman & Pinto 1993) coupled with our steadily improving knowledge of the distance scale out to ~ 50 Mpc will lead to elucidation of the appropriate thermonuclear explosion model. However, this will not be possible if better atomic data does not become available. This is the key improvement required for the field to progress.

Acknowledgements

We would especially like to thank Ron Eastman for helpful discussions regarding the spectral modelling. We are indebted to Alexei Filippenko for providing us with a contemporary optical spectrum of SN 1995D. Our thanks go to Jason Spyromilio for assisting with the the SN 1992G spectrum, for providing us with the +403 day optical spectrum of SN 1991T, and for many constructive comments in his rôle as referee. We much appreciate the staff at UKIRT for their excellent support. We thank John Pilkington of the RGO for measuring astrometric positions. The United Kingdom Infrared Telescope is operated by the Joint Astronomy Centre on behalf of the U.K. Particle Physics and Astronomy Research Council (PPARC). The Isaac Newton and William Herschel Telescopes are operated on the island of La Palma by the Royal Greenwich Observatory in the Spanish Observatorio del Roque de los Muchachos of the Instituto de Astrofísica de Canarias. EJC.B is supported by a PPARC studentship.

REFERENCES

- Aaronson M., Huchra J., Mould J., Schechter P.L., Tully R.B., 1982, *ApJ*, 258, 64
- Axelrod T.S., 1980a, Ph.D. thesis, UCRL-52994, University of California, Santa Cruz
- Axelrod T.S., 1980b, in J.C. Wheeler ed, *Type I Supernovae*, University of Texas, Austin, p80
- Barbon R., Cappellaro E., Turatto M., 1984, *A&A*, 135, 27
- Barbon R., Benetti S., Rosino L., Cappellaro E., Turatto, M., 1990, *A&A*, 237, 79
- Branch D., 1980, in Meyerott R., Gillespie G.H., eds, *Supernovae Spectra*, American Institute of Physics, New York, p39
- Cai W. & Pradhan A.K., 1993, *ApJ Suppl.*, 88, 329
- Cardelli J., Clayton G., Mathis J., 1989, *ApJ*, 345, 245
- Colgate S.A., McKee C., 1969, *ApJ*, 157, 623
- Colgate S.A., 1997, in Ruiz-Lapuente R., Canal R., Isern J., eds, *Thermonuclear Supernovae*, NATO ASI Series, p273
- Daly P.N., 1996, SUN/27, Starlink Project, CLRC
- Doggett J.B. & Branch D., 1985, *ApJ*, 90, 2303
- Eastman R.G. & Pinto P.A., 1993, *ApJ*, 412, 731
- Elias J.H., Frogel J.A., Hackwell J.A., Persson S.E., 1981, *ApJ*, 251, L13
- Elias J.H., Matthews K., Neugebauer G., Persson S.R., 1985, *ApJ*, 296, 379
- Evans R., 1986, *IAU Circ.* 4208
- Fairall A., 1986, *IAU Circ.* 4210
- Filippenko A.V., Richmond M.W., Matheson T., Shields J.C., Burbidge E.M., Cohen R.D., Dickinson M., Malkan M.A., Nelson B., Pietz J., Schlegel D., Schmeer P., Spinrad H., Steidel C.C., Tran H.D., Wren W., 1992 *ApJ*, 384, L15
- Frogel J.A., Gregory B., Kawara K., Laney D., Phillips M.M., Terndrup D., Vrba F., Whitford A.E., 1987, *ApJ*, 315, L129

Fuhr J.R., Martin G.A., Wiese W.L., 1988, Atomic Transition Probabilities, New York

Graham J.R., 1986, MNRAS, 220, 27p

Graham J.R., Baas F., Geballe T.R., Smith M.G., Longmore A.J., Williams P.M., 1987, preprint

Graham J.R., Wright G.S., Longmore A.J., 1987, ApJ, 313, 847

Hansen, 1984, ApJ, 277, 435

Heathcote D., Cowley A., Hutchings J., 1986, IAU Circ. 4210

Hill P.W., 1986, IAU Circ. 4210

Höflich P., Khokhlov A.M., Wheeler J.C., 1995, ApJ, 444, 831

Höflich P., Khokhlov A.M., 1996, ApJ, 457, 500

Hoyle F., Fowler W.A., 1960, ApJ, 132, 565

Hummer D.G., Berrington K.A., Eissner W., Pradhan A.K., Saraph H.E., Tully J.A., 1993, A&A, 279, 298

Iben I. & Tutukov A., 1984, ApJ Suppl, 55, 335

Jeffery D., Leibundgut B., Kirshner R.P., Benetti S., Branch D., Sonneborn G., 1992, ApJ, 397, 304

Khokhlov A.M., 1991a, A&A, 245, 114

Khokhlov A.M., 1991b, A&A, 245, L25

Kirshner R.P., Oke J.B., Penston M., Searle L., 1973, ApJ, 185, 303

Kirshner R.P. & Kwan J., 1975, ApJ, 197, 415

Kirshner R.P., 1986, IAU Circ. 4216

Kirshner R.P., Jeffery D.J., Leibundgut B., Challis P.M., Sonneborn G., Phillips M.M., Suntzeff N.B., Smith R.C., Winkler P.F., Winge C., Hamuy M., Hunter D.A., Roth K.C., Blades J.C., Branch D., Chevalier R.A., Fransson C., Panagia N., Wagoner R.V., Wheeler J.C., Harkness R.P., 1993, ApJ, 415, 589

Kuchner M.J., Kirshner R.P., Pinto P.A., Leibundgut B., 1994, ApJ, 426, L89

Kurucz R.L. & Peytremann E., 1975, SAO Special Report 362

Kurucz R.L., 1988, in McNally M., ed, Trans. IAU, XXB, Dordrecht: Kluwer, 168-172

Livne E., 1990, ApJ, 354, L53

Livne E., Glasner A.S., 1990, ApJ, 361, 244

Livne E. & Arnett D., 1995, ApJ, 452, 62

Lynch D.K., Rudy R.J., Rossano G.S., Erwin P., Puetter R.C., 1990, AJ, 100, 223

Lynch D.K., Erwin P., Rudy R.J., Rossano G.S., Puetter R.C., 1992, AJ, 104, 1156

Mazzali P.A., Danziger I.J., Turatto M., 1995, A&A, 297, 509

Meikle W.P.S., Bowers E.J.C., Pinto P.A., Eastman R.G., Cumming R.J., Geballe T.R., Lewis J.R., Walton N.A., 1997, in Canal R., Ruiz-Lapuente P., Isern J., eds, Proc. NATO Advanced Study Institute on Thermonuclear Supernovae, Kluwer, The Netherlands, p53

Meikle W.P.S., Cumming R.J., Geballe T.R., Lewis J.R., Walton N.A., Balcells M., Cimatti A., Croom S.M., Dhillon V.S., Economou F., Jenkins C.R., Knapen J.H., Lucey J.R., Meadows V.S., Morris P.W., Pérez-Fournon I., Shanks T., Smith L.J., Tanvir N.R., Veilleux S., Vilchez J., Wall J.V., 1996, MNRAS, 281, 263

Mendoza C. & Zeppen C.J., 1982, MNRAS, 198, 127

Mendoza C., 1983, in Proc. Symposium on Planetary Nebulae, Dordrecht, London, England, p143-172

Meyerott R.E., 1980, ApJ, 239, 257

Meurer G., 1986, AUC Circ. 4216

Nahar S.N. & Pradhan A.K., 1996, A&A, 119, 509

Nomoto K., Thielemann F-K., Yokoi K., 1984, ApJ, 286, 644

Nugent P., Baron E., Hauschildt P.H., Branch D., 1994, BAAS, 185, 7902

Nussbaumer H. & Storey P.J., 1988a, A&A, 200, L25

Nussbaumer H. & Storey P.J., 1988b, A&A, 193, 327

Pankey T., 1962, Ph.D. thesis, Howard University

Pelan J. & Berrington K.A., 1996, preprint

Phillips M. & Geisler D., 1986, IAU Circ. 4210

Phillips M. & Hamuy M., 1991, IAU Circ. 5239

Phillips M.M., Phillips A.C., Heathcote S.R., Blanco V.M., Geisler D., Hamilton D., Suntzeff N.B., Jablonski F.J., Steiner J.E., Gowley A.P., 1987, PASP, 99, 592

Phillips M.M., Wells L.A., Suntzeff N.B., Hamuy M., Leibundgut B., Kirshner R.P., Foltz C.B., 1992, AJ, 103, 1632

Phillips M.M., 1993, ApJ, 413, L105

Pradhan A.K. & Zhang H.L., 1993, ApJ, 409, L77

Reiss A.G., Press W.H., Kirshner R.P., 1995, ApJ, 438, L17

Ruiz-Lapuente P., 1992, Ph.D. thesis, University of Barcelona

Schlegel E.M., 1995, ApJ, 109, 2620

Shortridge K., 1995, Starlink Project, CLRC

Sobolev V.V., 1960, Moving Envelopes of Stars, Harvard University

Spyromilio J., Meikle W.P.S., Allen D.A., Graham J.R., 1992, MNRAS, 258, 53p

Spyromilio J., Pinto P.A., Eastman R.G., 1994, MNRAS, 266, L17

Thielemann F-K., Nomoto., Yokoi., 1986, A& A, 158, 17

Tonry J. & Strauss M., 1986, IAU Circ. 4210

Van Den Bergh S., 1996, PASP, 108, 1091

Varani G-F., Meikle, W.P.S., Spyromilio J., Allen D.A., 1990, MNRAS, 245, 570

Wamsteker W., Gilmozzi R., Gry C., Machetto F., Panagia N., 1986, IAU Circ. 4216

Weaver J.C., Swartz D.A., & Harkness R.P., 1993, Phys. Rep., 227, 113

Wells L.A., Phillips M.M., Suntzeff N.B., Heathcote S.R., Hamuy M., Navarrete M., Fernandez M., Weller W.G., Schammer R.A., 1994, AJ, 108, 2234

Woosley S.E., Weaver T.A., 1994a, in Bludman S., Mochkovitch R., Zinn-Justin J., eds, Proc. Les Houches Session LIX, Elsevier Science, Paris, p.63

Woosley S.E. & Weaver T.A., 1994b, ApJ, 423, 371

Zhang H.L. & Pradhan A.K., 1995, ApJ, 293, 953

Zhang H.L. & Pradhan A.K., 1995, J.Phys.B: At. Mol. Opt. Phys., 28, 3403

Zhang H.L., 1996, A&A, 119, 523

Table 1: Type Ia supernovae observed spectroscopically in the infrared

SN	Parent Galaxy	Position (2000.0)		Offset from Gal. nucl.	Discovery Date	Vmax	t_{Bmax}	Discovery IAU Circular
		RA (hr min sec)	Dec (deg amin asec)	(asec)				
1986G	NGC 5128	13 25 36.55	-43 01 51.7	120E 60S	3-05-86	11.4	11-05-86	4208
1991T	NGC 4527	12 34 10.18	+02 39 56.79	26E 45N	13-04-91	11.5	28-04-91	5239
1992G	NGC 3294	10 36 16.52	+37 19 13.7	27E 10.5S	9-02-92	13.7	20-02-92	5452
1994ae	NGC 3370	10 47 01.99	+17 16 32.1	30.3W 6.1N	14-11-94	12.5	27-11-94	6105
1995D	NGC 2962	09 40 54.80	+05 08 26.7	11E 90.5S	10-2-94	13.4	17-02-95	6134
1995al	NGC 3021	09 53 53.02	+33 18 58.7	15.0W 2.9S	1-11-95	13.0	30-10-95	6255
1996X	NGC 5061	13 20 46.44	-27 06 28.1	52W 31S	12-4-96	13.2	13-04-96	6380

Table 2: Log of infrared spectroscopy

Source	Date UT	Epoch (d)	Telescope/Instrument	$\lambda\lambda$ (μm)	Resolution (kms^{-1})
SN1986G	1986 May 24	+13	UKIRT/CGS2	1.056–1.822	500
				1.935–2.487	500 ^a
	1986 June 10	+30	UKIRT/CGS2	1.079–1.356	500
SN1991T	1991 June 26	+60	AAT/IRIS	1.945–2.517	500 ^b
				0.90–1.31	500
				1.41–1.80	800
	1992 Mar 31	+338	UKIRT/CGS4	1.91–2.45	550
				1.18–1.36	800
				1.42–1.8	800
				2.07–2.46	800
SN1992G	1992 Mar 30	+39	UKIRT/CGS4	1.0–1.8	600
SN1994ae	1995 May 20	+175	UKIRT/CGS4	1.0–1.35	200
	1995 May 19	+174		1.43–2.09	240
SN 1995D	1995 May 20	+92	UKIRT/CGS4	1.015–1.224	350
	1995 May 19	+91		1.43–2.09	400
	1995 May 21	+93		1.94–2.50	350
SN1995al	1996 Feb 6	+94	UKIRT/CGS4	1.0–1.34	250
				1.42–2.08	600
	1996 Apr 28	+176	UKIRT/CGS4	0.985–1.30	1000 ^c
				1.49–1.80	400 ^d
	1996 Apr 29	+177		2.135–2.470	350
SN1996X	1996 Apr 29	+19	UKIRT/CGS4	0.995–1.30	300
				1.445–1.77	300
				1.97–2.138	200

^aThe J, H and K observations which make up most of the ‘day +13’ spectrum were actually obtained on days +12, +13 and +14 respectively. Smaller fill-in sections were obtained on day +18 (1.767–1.822 μm , 1.935–1.971 μm) and day +22 (1.361–1.484 μm). The 1.361–1.484 μm section was taken with a CVF.

^bIn the ‘day +30’ spectrum the 1.079–1.356 μm section was taken on day +30, while the 1.945–2.517 μm was taken on day +31.

^cThe J spectra were made up of observations taken on days +175, +176 and +177.

^dThe H spectra were made up of observations taken on days +175 and +176.

Table 3: Log of optical spectroscopy

Source	Date UT	Epoch (d)	Telescope/Instrument	$\lambda\lambda$ (μm)	Resolution (kms^{-1})
SN1991T	1991 June 26	+60	AAT/Cass. spectrograph	0.38–0.95	900
SN1991T	1992 June 4	+403	AAT/Cass. spectrograph	0.32–1.00	900
SN1992G	1992 Mar 8	+17	INT/FOS	0.37–1.00	600 (1st ord) 800 (2nd ord)
SN1994ae	1995 Feb 23	+89	WHT/ISIS	0.34–0.92	300
SN1995D	1995 May 24	+96	Lick/Shane 3-m	0.31–1.04	200
SN1995al	1996 Apr 1	+149	INT/IDS	0.365–0.90	600

Table 4: Fixed Parameters for the Spectral Synthesis Model Fits

Source	Epoch (d)	D (Mpc)	Z	Av	$N_{Co^+}/$ N_{Fe^+}
SN 1995D	92	27.0 ± 3.2	1.0065	0.6 ± 0.1	0.66
SN 1995al	94	23.8 ± 2.9	1.005	0.8 ± 0.1	0.66
	174				0.25
SN 1994ae	173	21.8 ± 2.6	1.004	0.2 ± 0.2	0.25
SN 1991T	338	14.4 ± 1.7	1.0058	0.66 ± 0.23	0.04

Table 5: Variable Parameters for the Spectral Synthesis Model Fits

Source	T_e (K)	N_{Fe+Co}^a (cm^{-3})	neutral atom fraction	singly ionized fraction	doubly ionized fraction	N_S^b (cm^{-3})	$N_{S^+}/$ $N_{S^{2+}}$	V_{exp}^c ($\times 10^3 \text{kms}^{-1}$)
SN 1995D Figs 4, 5 & 6	7000	3.9e6	0.2	0.2	0.6	7e5	0.5	8.0
SN 1995al at 94d Fig 7	7000	6.5e6	0.1	0.1	0.8	7e5	0.5	8.5
SN 1995al at 176d Figs 8 & 9	6000	5.8e5	—	0.1	0.9	1.5e5	0.5	8.5
SN 1994ae Fig 10	6000	3e5	0.1	0.2	0.7	8.8e4	0.5	8.5
SN 1991T Figs 11 & 12	5600	1.7e5	0.01	0.15	0.84	—	—	8.5

^aTotal iron and cobalt ion density^bTotal sulphur ion density^cExpansion velocity of supernova ejecta

Table 6: Modelled Optical Emission Features of SNe Spectra

λ_{rest}^a	Identification	SN 1995D +92d		SN 1995al +176d		SN 1991T +363d	
		Line Flux ^b	λ_{peak}^a	Line Flux ^b	λ_{peak}^a	Line Flux ^b	λ_{peak}^a
0.4069 ^c	[SII] $3p^3 \ ^2P_{3/2}-3p^3 \ ^4S_{3/2}$	—	—	13.4	0.4095	—	—
0.4078 ^c	[S II] $3p^3 \ ^2P_{1/2}-3p^3 \ ^4S_{3/2}$	—	—	3.43	—	—	—
0.4251 ^d	[Fe II] $a^4F_{5/2}-b^2H_{9/2}$	31.9	0.4459	0.08	0.4420	0.38	0.4385
0.4277 ^d	[Fe II] $a^4F_{7/2}-a^4G_{9/2}$	17.7	—	2.00	—	4.84	—
0.4358 ^d	[Fe II] $a^4F_{3/2}-a^4G_{5/2}$	11.2	—	1.29	—	3.12	—
0.4359 ^d	[Fe II] $a^6D_{7/2}-a^6S_{5/2}$	22.3	—	2.36	—	6.04	—
0.4356 ^d	[Fe II] $a^4F_{5/2}-b^2P_{3/2}$	0.12	—	0.02	—	0.08	—
0.4411 ^d	[Co II] $a^3F_2-b^3P_1$	5.93	—	0.32	—	0.18	—
0.4414 ^d	[Fe II] $a^6D_{5/2}-a^6S_{5/2}$	16.2	—	1.72	—	4.39	—
0.4416 ^d	[Fe II] $a^6D_{9/2}-b^4F_{9/2}$	23.6	—	3.05	—	7.92	—
0.4658 ^e	[Fe III] $a^5D_4-^3F_{24}$	129	0.4705	49.3	0.4715	87.7	0.4718
0.4702 ^e	[Fe III] $^5D_3-^3F_3$	58.6	—	25.7	—	47.6	—
0.4989 ^f	[Fe III] $^5D_3-^3F_4$	—	—	1.06	0.5032	—	—
0.5006 ^f	[FeII] $a^4F_{5/2}-b^4F_{7/2}$	—	—	0.39	—	—	—
0.5007 ^f	[Fe II] $a^6D_{3/2}-b^4P_{5/2}$	—	—	0.20	—	—	—
0.5159 ^g	[Fe II] $a^4F_{7/2}-b^4P_{3/2}$	41.0	0.5305	6.96	0.5292	21.1	0.5295
0.5270 ^g	[Fe III] $a^5D_3-a^3P_{22}$	100	—	36.0	—	63.1	—
0.5890 ^h	[Co III] $a^4F_{9/2}-a^2G_{9/2}$	181	0.5930	34.6	0.5920	13.4	0.5920
0.5908 ^h	[Co III] $a^4F_{7/2}-a^2G_{7/2}$	53.2	—	11.8	—	4.85	—
0.6129 ⁱ	[CoIII] $a^4F_{5/2}-a^2G_{7/2}$	37.6	0.6218	8.36	0.6210	3.42	0.6195
0.6197 ⁱ	[Co III] $a^4F_{7/2}-a^2G_{9/2}$	51.7	—	9.88	—	3.83	—
0.6578	[Co III] $a^4F_{9/2}-a^4P_{5/2}$	24.6	0.6622	9.10	0.6620	5.28	0.6620
0.7155 ^j	[Fe II] $a^4F_{9/2}-a^2G_{9/2}$	31.2	0.7220	11.0	0.7195	52.8	0.7205
0.7172 ^j	[Fe II] $a^4F_{7/2}-a^2G_{7/2}$	10.9	—	4.82	—	28.5	—
0.7388 ^k	[Fe II] $a^4F_{5/2}-a^2G_{7/2}$	8.15	0.7565	3.59	0.7500	21.3	0.7470
0.7453 ^k	[Fe II] $a^4F_{7/2}-a^2G_{9/2}$	9.59	—	3.37	—	16.2	—
0.7541 ^k	[Co II] $a^3F_4-a^3P_2$	23.5	—	2.96	—	2.61	—
0.8029	[Co II] $a^3F_3-a^3P_1$	10.1	0.8150	1.29	0.8092	—	—
0.8617	[Fe II] $a^4F_{9/2}-a^4P_{5/2}$	—	—	2.57	0.8662	16.3	0.8680

^a λ is in microns

^bLine flux is $\times 10^{-15} \text{erg s}^{-1} \text{cm}^{-2}$

^cBlend of two lines

^dBlend of eight lines

^eBlend of two lines

^fBlend of three lines

^gBlend of two lines

^hBlend of two lines

ⁱBlend of two lines

^jBlend of two lines

^kBlend of three lines

Table 7: Modelled Infrared Emission Features of SNe Spectra at $t < 100$ days

λ_{rest}^a	Identification	SN1995D		SN1995al	
		Line Flux ^b	λ_{peak}^a	Line Flux ^b	λ_{peak}^a
0.9345 ^c	[Co II] $a^3F_3 - a^1D_2$	25.6	0.9570	—	—
0.9531 ^c	[S III] $3p^2 \ ^1D_2 - 3p^2 \ ^3P_2$	80.0	—	—	—
1.0191 ^d	[Co II] $a^3F_4 - b^3F_4$	14.4	1.033	19.2	1.036
1.0283 ^d	[Co II] $a^3F_2 - b^3F_2$	4.56	—	6.17	—
1.0289 ^d	[S II] $3p^2 \ ^2P_{3/2} - 3p^3 \ ^2D_{3/2}$	7.91	—	13.9	—
1.0323 ^d	[S II] $3p^2 \ ^2P_{3/2} - 3p^3 \ ^2D_{5/2}$	13.3	—	23.4	—
1.0339 ^d	[S II] $3p^2 \ ^2P_{1/2} - 3p^3 \ ^2D_{5/2}$	6.31	—	10.8	—
1.0373 ^d	[S II] $3p^2 \ ^2P_{1/2} - 3p^3 \ ^2D_{5/2}$	2.51	—	4.30	—
1.2567 ^e	[Fe II] $a^6D_{9/2} - a^4D_{7/2}$	2.86	1.279	3.69	1.280
1.2723 ^e	[Co III] $a^4P_{5/2} - a^2D_{5/2}$	1.39	—	6.45	—
1.443	[Fe I] $a^5D_4 - a^5F_5$	1.71	1.452	3.30	1.449
1.5474 ^f	[Co II] $a^5F_5 - b^3F_4$	7.11	1.558	9.53	1.556
1.5489 ^f	[Co III] $a^2G_{9/2} - a^2H_{9/2}$	7.28	—	29.1	—
1.6435 ^g	[Fe II] $a^4F_{9/2} - a^4D_{7/2}$	2.11	1.649	2.72	1.646
1.6348 ^g	[Co II] $a^5F_1 - b^3F_2$	1.57	—	2.12	—
1.7366 ^h	[Co II] $a^5F_2 - b^3F_3$	1.45	1.755	1.96	1.756
1.7416 ^h	[Co III] $a^2G_{9/2} - a^2H_{11/2}$	3.18	—	12.2	—
1.7643 ^h	[Co III] $a^2G_{7/2} - a^2H_{9/2}$	1.92	—	7.67	—
1.9571 ⁱ	[Co III] $a^4P_{1/2} - a^2P_{1/2}$	2.95	2.008	11.8	1.997
1.9810 ⁱ	[Fe I] $a^5F_5 - a^3F_4$	2.46	—	3.26	—
2.0015 ⁱ	[Co III] $a^4P_{5/2} - a^2P_{3/2}$	4.62	—	19.2	—
2.0967 ^j	[Co III] $a^4P_{3/2} - a^2P_{3/2}$	2.36	2.110	—	—
2.1457 ^j	[Fe III] $a^3H_4 - a^3G_3$	1.28	—	—	—
2.2184 ^k	[Fe III] $a^3H_6 - a^3G_5$	2.36	2.248	—	—
2.2427 ^k	[Fe III] $a^3H_4 - a^3G_4$	2.04	—	—	—
2.2799 ^k	[Co III] $a^4P_{1/2} - a^2P_{3/2}$	0.89	—	—	—

^a λ is in microns

^bLine flux is $\times 10^{-15} \text{erg s}^{-1} \text{cm}^{-2}$

^cBlend of two lines

^dBlend of six lines

^eBlend of two lines

^fBlend of two lines

^gBlend of two lines

^hBlend of three lines

ⁱBlend of three lines

^jBlend of two lines

^kBlend of three lines

Table 8: Modelled Infrared Emission Features of SNe Spectra at $t > 100$ days

λ_{rest}^a	Identification	SN 1995al +176d		SN 1994ae +175d		SN 1991T +363d	
		Line Flux ^b	λ_{peak}^a	Line Flux ^b	λ_{peak}^a	Line Flux ^b	λ_{peak}^a
1.0191 ^c	[Co II] a^3F_4 - b^3F_4	2.61	1.0355	2.48	1.030	—	—
1.0283 ^c	[Co II] a^3F_2 - b^3F_2	0.76	—	0.71	—	—	—
1.0289 ^c	[S II] $3p^2\ ^2P_{3/2}$ - $3p^3\ ^2D_{3/2}$	3.19	—	1.28	—	—	—
1.0323 ^c	[S II] $3p^2\ ^2P_{3/2}$ - $3p^3\ ^2D_{5/2}$	5.34	—	2.14	—	—	—
1.0339 ^c	[S II] $3p^2\ ^2P_{1/2}$ - $3p^3\ ^2D_{5/2}$	2.91	—	0.51	—	—	—
1.0373 ^c	[S II] $3p^2\ ^2P_{1/2}$ - $3p^3\ ^2D_{5/2}$	1.16	—	0.58	—	—	—
1.2567 ^d	[Fe II] $a^6D_{9/2}$ - $a^4D_{7/2}$	1.84	1.269	2.21	1.264	14.6	1.267
1.2723 ^d	[Co III] $a^4P_{5/2}$ - $a^2D_{5/2}$	0.18	—	0.04	—	0.05	—
1.443	[Fe I] a^5D_4 - a^5F_5	—	—	0.96	1.448	0.89	1.451
1.5474 ^e	[Co II] a^5F_5 - b^3F_4	1.29	1.555	1.23	1.550	1.52	1.547
1.5489 ^e	[Co III] $a^2G_{9/2}$ - $a^2H_{9/2}$	1.53	—	0.43	—	0.63	—
1.6435 ^f	[Fe II] $a^4F_{9/2}$ - $a^4D_{7/2}$	1.36	1.651	1.63	1.649	10.8	1.654
1.6348 ^f	[Co II] a^5F_1 - b^3F_2	0.26	—	0.24	—	0.29	—
1.7366 ^g	[Co II] a^5F_2 - b^3F_3	0.25	1.754	0.23	1.749	0.28	1.812
1.7416 ^g	[Co III] $a^2G_{9/2}$ - $a^2H_{11/2}$	0.87	—	0.31	—	0.47	—
1.7643 ^g	[Co III] $a^2G_{7/2}$ - $a^2H_{9/2}$	0.40	—	0.11	—	0.17	—
1.8000 ^h	[Fe II] $a^4F_{5/2}$ - $a^4D_{5/2}$	—	—	0.31	1.8045	2.01	—
1.8094 ^h	[Fe II] $a^4F_{7/2}$ - $a^4D_{7/2}$	—	—	0.33	—	2.17	—
1.9571 ⁱ	[Co III] $a^4P_{1/2}$ - $a^2P_{1/2}$	—	—	0.18	1.992	—	—
1.9810 ⁱ	[Fe I] a^5F_5 - a^3F_4	—	—	0.69	—	—	—
2.0015 ⁱ	[Co III] $a^4P_{5/2}$ - $a^2P_{3/2}$	—	—	0.21	—	—	—
2.1457	[Fe III] a^3H_4 - a^3G_3	—	—	—	—	1.85	2.154
2.2184 ^j	[Fe III] a^3H_6 - a^3G_5	1.38	3.243	—	—	3.46	2.164
2.2427 ^j	[Fe III] a^3H_4 - a^3G_4	1.26	—	—	—	3.09	—
2.3485	[Fe III] a^3H_5 - a^3G_5	—	—	—	—	2.15	2.362

^a λ is in microns

^bLine flux is $\times 10^{-15}$ erg s⁻¹ cm⁻²

^cBlend of six lines

^dBlend of two lines

^eBlend of two lines

^fBlend of two lines

^gBlend of three lines

^hBlend of two lines

ⁱBlend of three lines

^jBlend of two lines

Table 9: Evolution of cobalt/iron mass ratio

Source	Epoch (d)	M_{Co}/M_{Fe}^a
SN 1995D	+92	0.66 ± 0.36
SN 1995al	+94	$0.66^{+0.6}_{-0.3}$
SN 1995al	+176	$0.25^{+0.25}_{-0.125}$
SN 1994ae	+175	$0.25^{+0.7}_{-0.07}$
SN 1991T	+338	0.04 ± 0.015

^aMass ratio values are as predicted by the ^{56}Ni decay hypothesis. The errors indicate the range of mass ratio over which a satisfactory model fit to the data was achieved. Most of this was due to atomic data uncertainties.

Table 10: Absolute mass estimates

Source	Epoch (d)	M_{Fe^0} (M_{\odot})	M_{Fe^+} (M_{\odot})	$M_{Fe^{2+}}$ (M_{\odot})	$M_{Fe^{3+}}^a$ (M_{\odot})	M_{Co^0} (M_{\odot})	M_{Co^+} (M_{\odot})	$M_{Co^{2+}}$ (M_{\odot})	$M_{Co^{3+}}^a$ (M_{\odot})	$M_{^{56}\text{Ni}}^b$ (M_{\odot})
SN 1995D	+92	<0.040	0.040	0.120	(0.022)	<0.027	0.027	0.081	(0.015)	0.27 ± 0.16
SN 1995al	+94	<0.040	0.040	0.32	(0.044)	<0.027	0.027	0.21	(0.030)	$0.67^{+1.1}_{-0.4}$
SN 1995al	+176	—	0.025	0.22	(0.078)	—	0.006	0.054	(0.019)	0.31 ± 0.19
SN 1994ae	+174	<0.013	0.026	0.090	(0.040)	<0.003	0.006	0.022	(0.010)	$0.14^{+0.5}_{-0.05}$
SN 1991T	+363	<0.0055	0.082	0.46	(0.31)	<0.00026	0.004	0.022	(0.015)	0.57 ± 0.14

^aThe mass of triply-ionized material is determined using Axelrod’s estimates.

^bThe values for the total ^{56}Ni mass are conservative as they are obtained by summing the singly- and doubly- ionized iron and cobalt only. Inclusion of neutral and triply-ionized species would increase the total mass by a factor of 1.5–2.5.

^cOwing to the low signal-to-noise the error here is a factor of 1.5 times larger than for the other supernovae.

Figure Captions

Figure 1: Photospheric phase infrared spectra of SNe 1986G, 1992G, 1991T and 1996X arranged by epoch, relative to t_{Bmax} (see Table 2 for details). Each spectrum has been wavelength-shifted to the rest frame of the parent galaxy. No reddening correction has been applied. For clarity, all of the spectra have been displaced vertically. The dotted horizontal lines on the left side indicate zero flux for each of the spectra. For SN 1991T zero flux is at the x-axis. The fluxes have also been multiplied by different factors (shown in brackets) to allow comparison of the features at the different epochs.

Figure 2: Nebular phase infrared spectra of SNe 1991T, 1994ae, 1995D and 1995al arranged by epoch. Otherwise as described in Figure 1 caption.

Figure 3: Optical spectra of SNe 1992G, 1991T, 1994ae, 1995D and 1995al arranged by epoch, relative to t_{Bmax} (see Table 3 for details). For SN 1991T at +403 d zero flux is at the x-axis. Other details as described in Figure 1 caption.

Figure 4: Optical spectrum (solid line) of SN 1995D at +96 days, obtained at the Shane 3 m telescope of Lick Observatory (see Table 3 for details). It has not been wavelength-corrected for redshift, nor de-reddened. Also shown is our best model match (dashed line) (see Table 5) which has been red-shifted and reddened to match the SN. The same model parameters are used for the day +92 NIR model spectrum shown in Fig. 5. Features we believe to be predominantly due to cobalt or iron are indicated.

Figure 5: Near-infrared spectrum (solid line) of SN 1995D at +92 days, obtained at the United Kingdom Infrared Telescope with the cooled grating spectrometer CGS4 (see Table 2 for details). It has not been wavelength-corrected for redshift, nor de-reddened. Also shown is our best model match (dashed line) (see Table 5) which has been red-shifted and reddened to match the SN. The same model parameters are used for the optical model spectrum shown in Fig. 4. Features we believe to be predominantly due to cobalt, iron or sulphur are indicated.

Figure 6: As Figure 5 but showing in detail the features in the wavelength range 1.5–2.5 μm .

Figure 7: Near-infrared spectrum (solid line) of SN 1995al at +94 days, obtained at the United Kingdom Infrared Telescope with the cooled grating spectrometer CGS4 (see Table 2 for details). Other details as described in Figure 5 caption.

Figure 8: Optical spectrum (solid line) of SN 1995al at +149 days, obtained with the intermediate dispersion spectrograph of the Isaac Newton Telescope, La Palma (see Table 3 for details). It has been scaled to correspond approximately to the epoch of the day +176 NIR spectrum. The same model parameters are used for the day +176 NIR model spectrum shown in Fig.9. Other details as described in Figure 4 caption.

Figure 9: Near-infrared spectrum (solid line) of SN 1995al at +176 days, obtained at

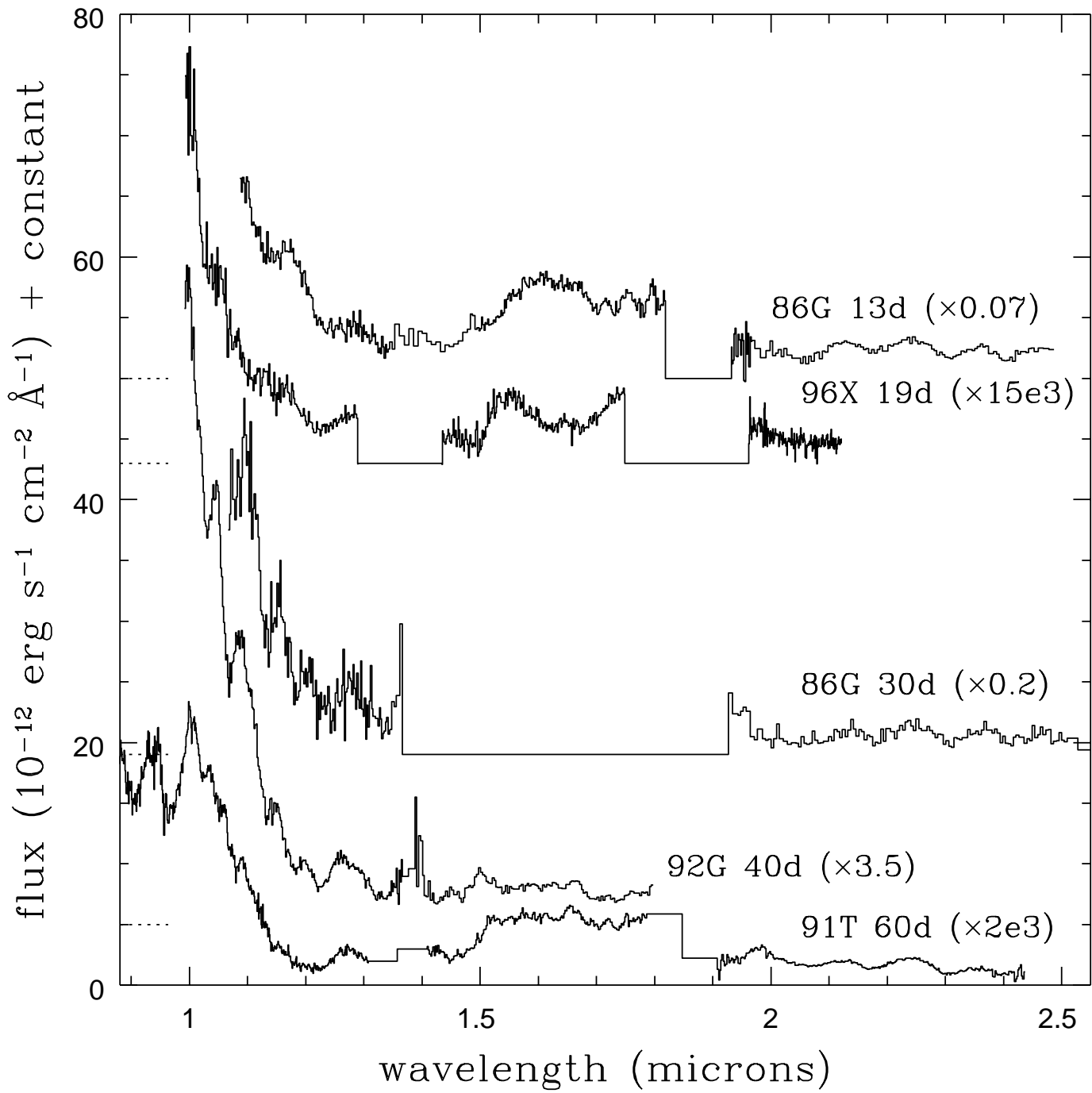
the United Kingdom Infrared Telescope with the cooled grating spectrometer CGS4 (see Table 2 for details). Other details as described in Figure 5 caption.

Figure 10: Near-infrared spectrum (solid line) of SN 1994ae at +175 days, obtained at the United Kingdom Infrared Telescope with the cooled grating spectrometer CGS4 (see Table 2 for details). To improve signal-to-noise, the spectrum has been binned by a factor of $\times 4$. Other details as described in Figure 5 caption.

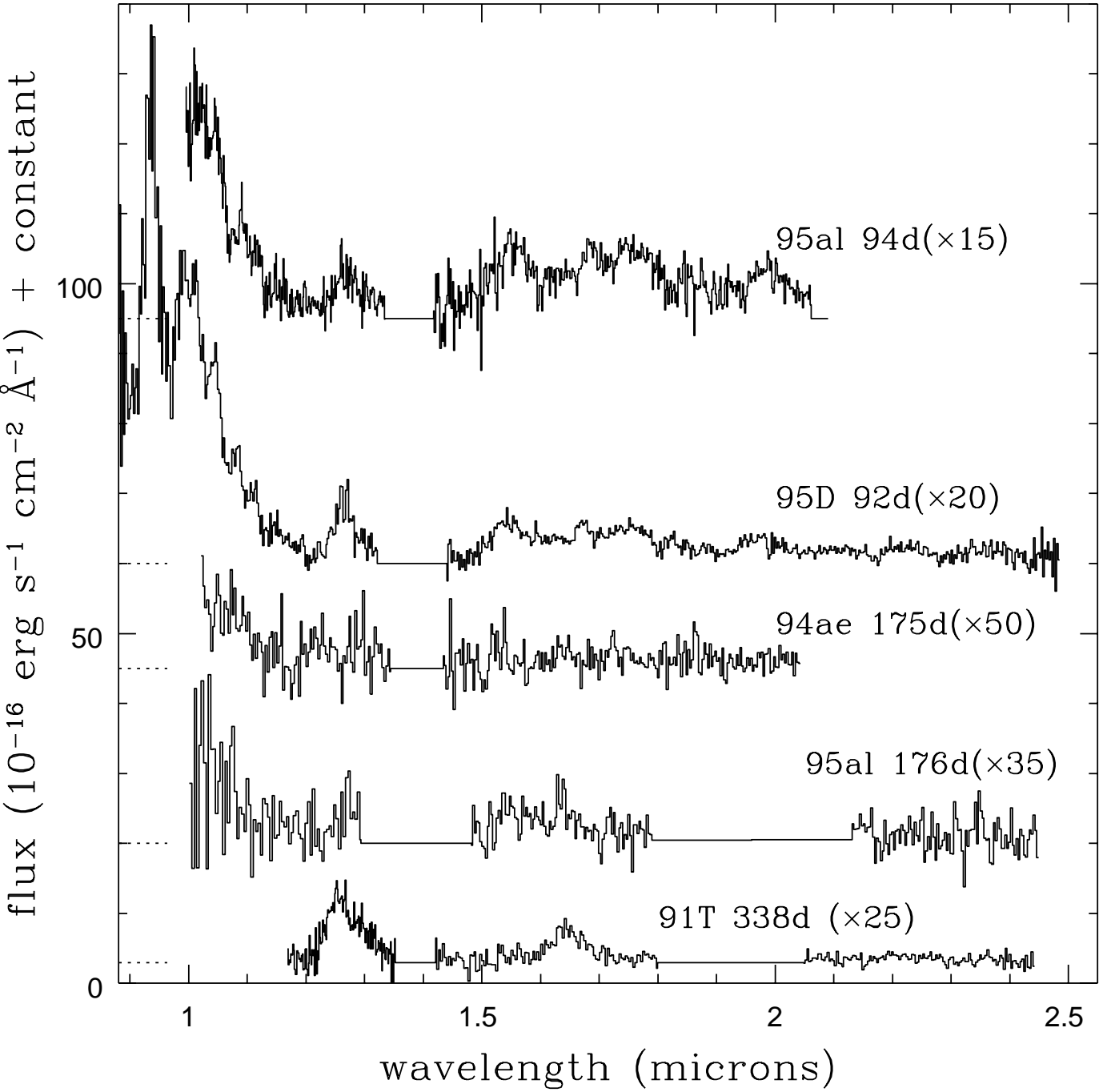
Figure 11: Optical spectrum (solid line) of SN 1991T at +403 days, obtained with the Cassegrain spectrograph on the Anglo-Australian Telescope (see Table 3 for details). The flux has been scaled to approximately the epoch of the +338 day near-infrared spectrum (Fig. 12). The same model parameters are used for the day +338 NIR model spectrum shown in Fig. 12. Other details as described in Figure 4 caption.

Figure 12: Near-infrared spectrum (solid line) of SN 1991T at +338 days, obtained at the United Kingdom Infrared Telescope with the cooled grating spectrometer CGS4 (see Table 2 for details). Other details as described in Figure 5 caption.

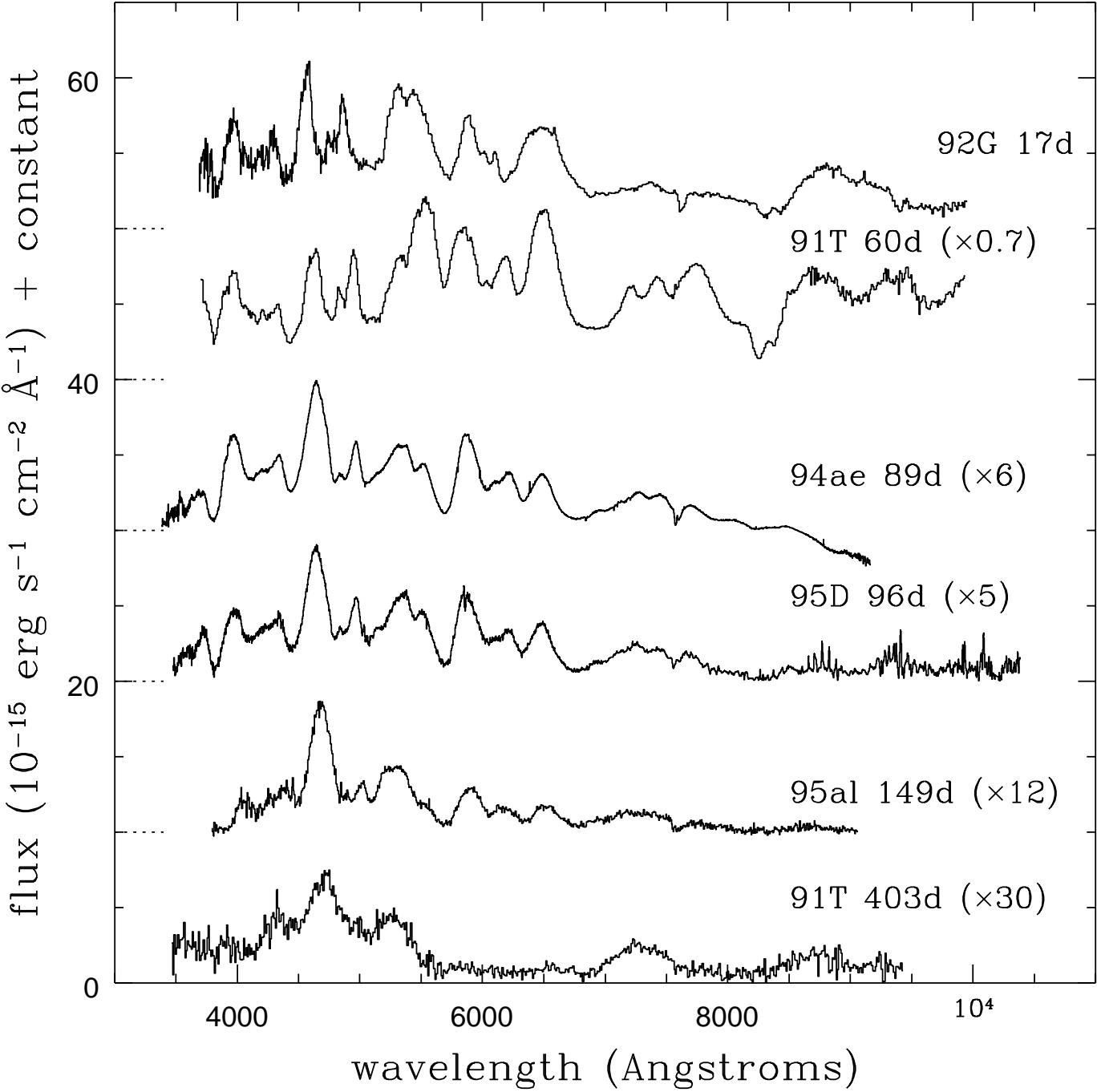
Type Ia Supernovae – evolution of IR spectra



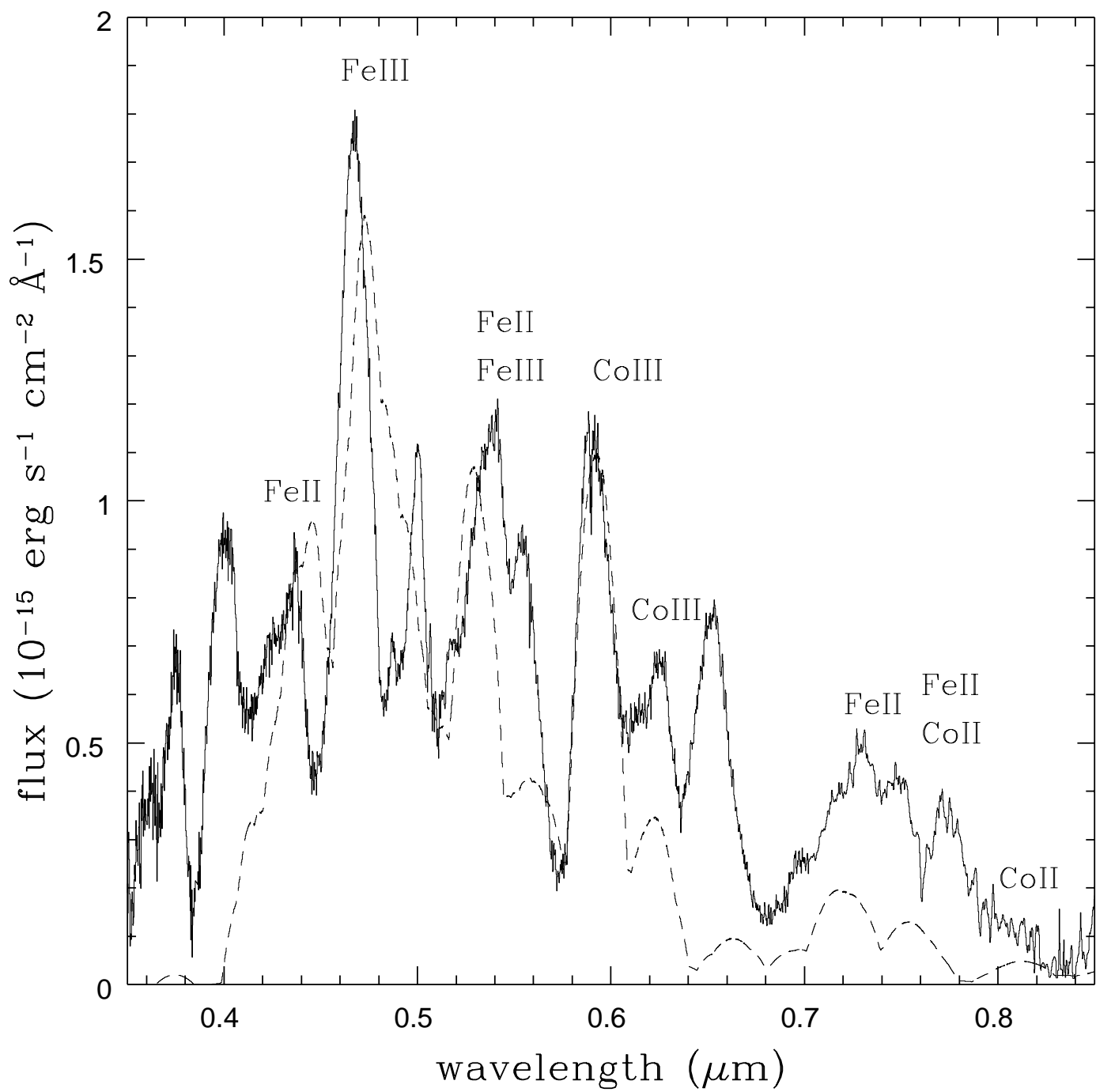
Type Ia Supernovae – evolution of IR spectra



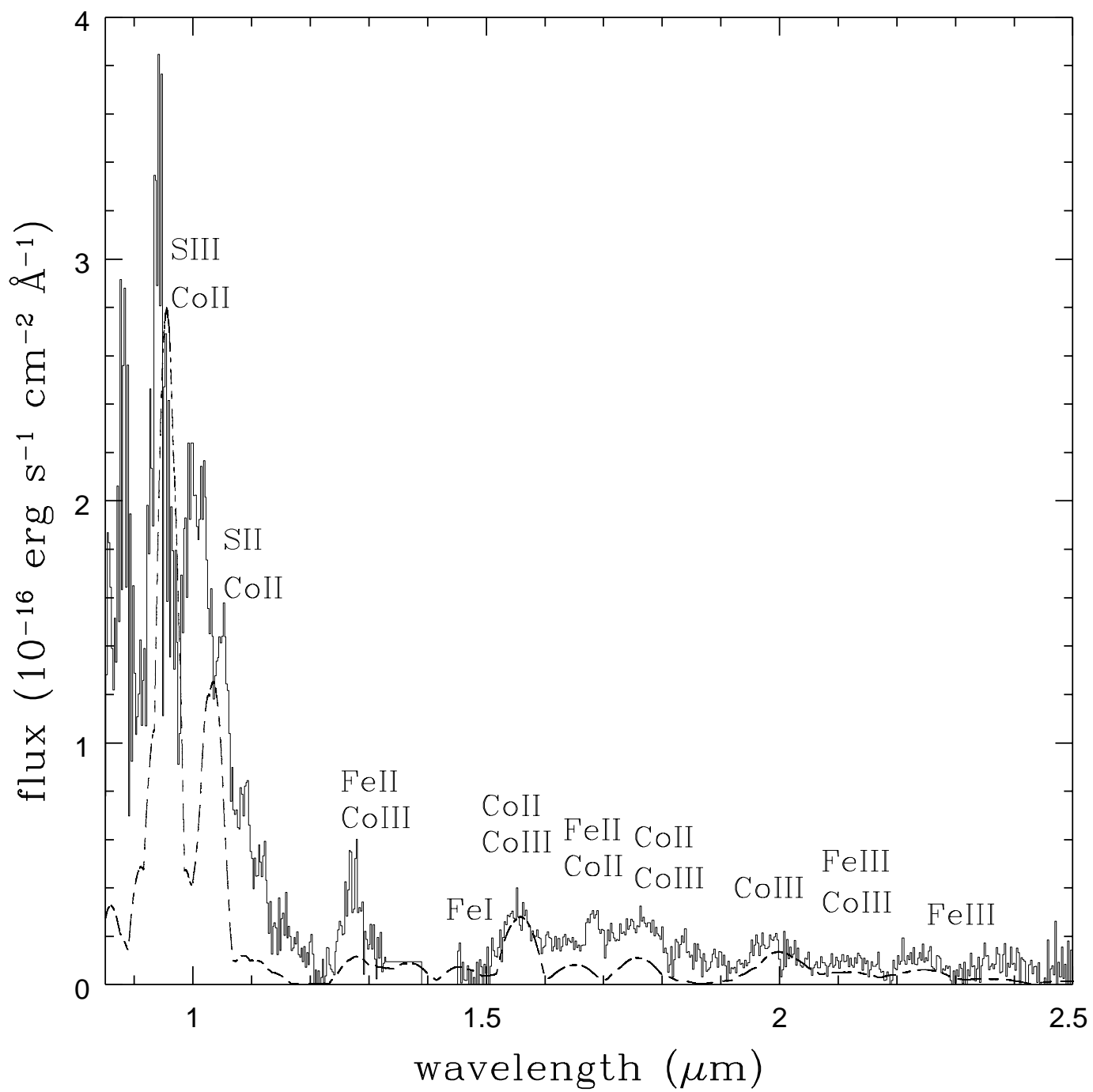
Type Ia Supernovae – evolution of optical spectra



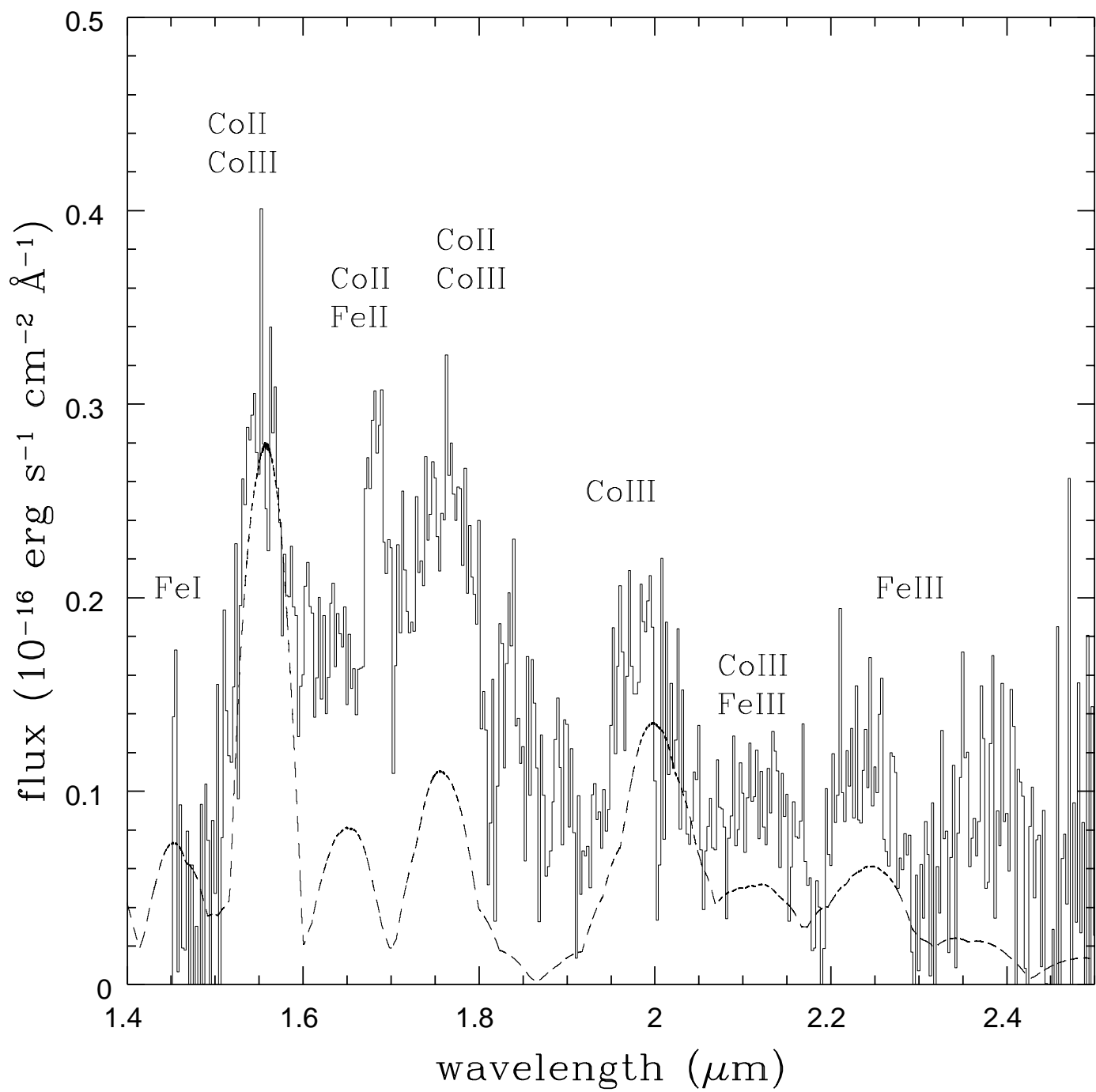
MODEL FIT OF SN 1995D AT 92-DAY EPOCH



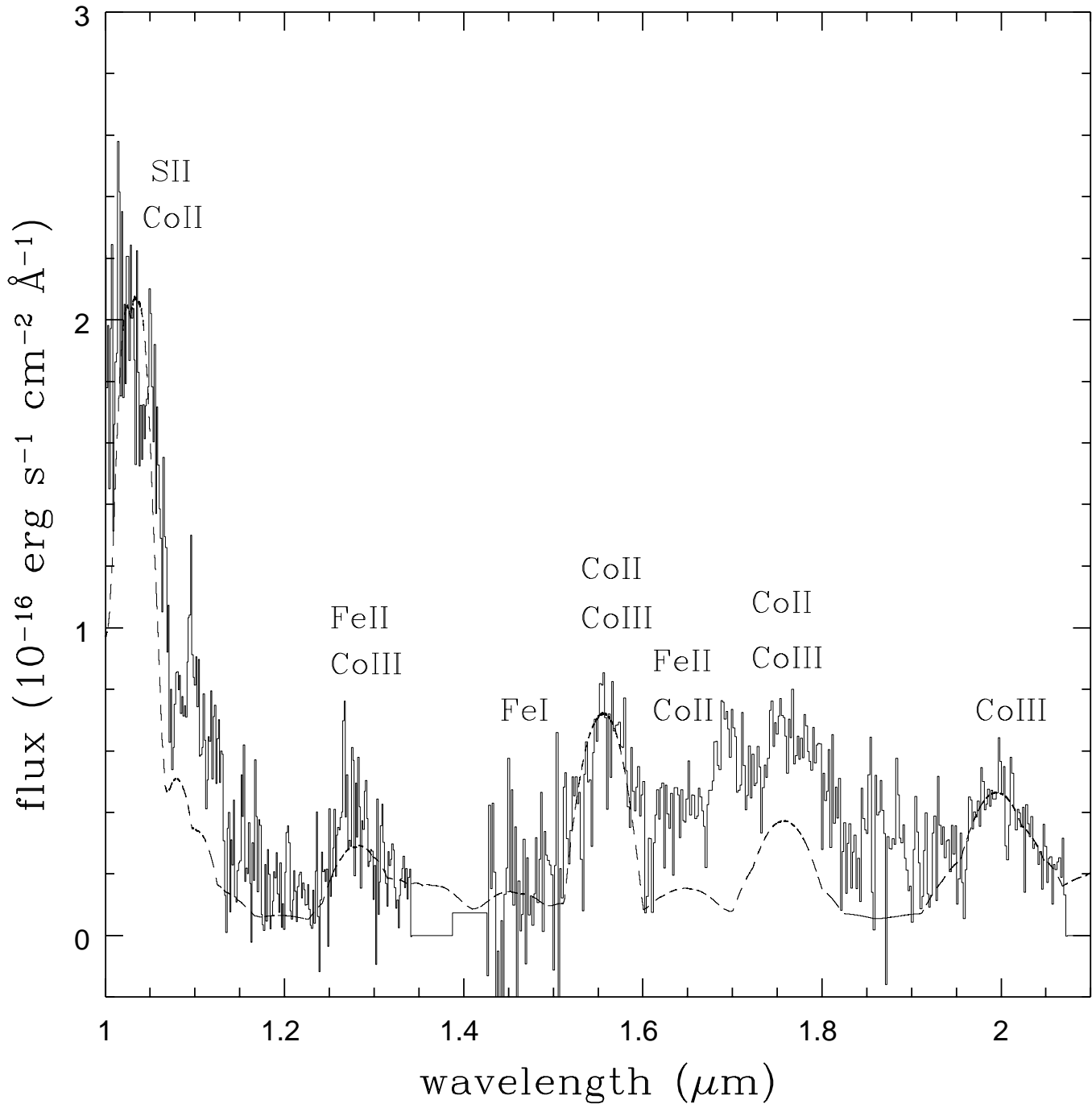
MODEL FIT OF SN 1995D AT 92-DAY EPOCH



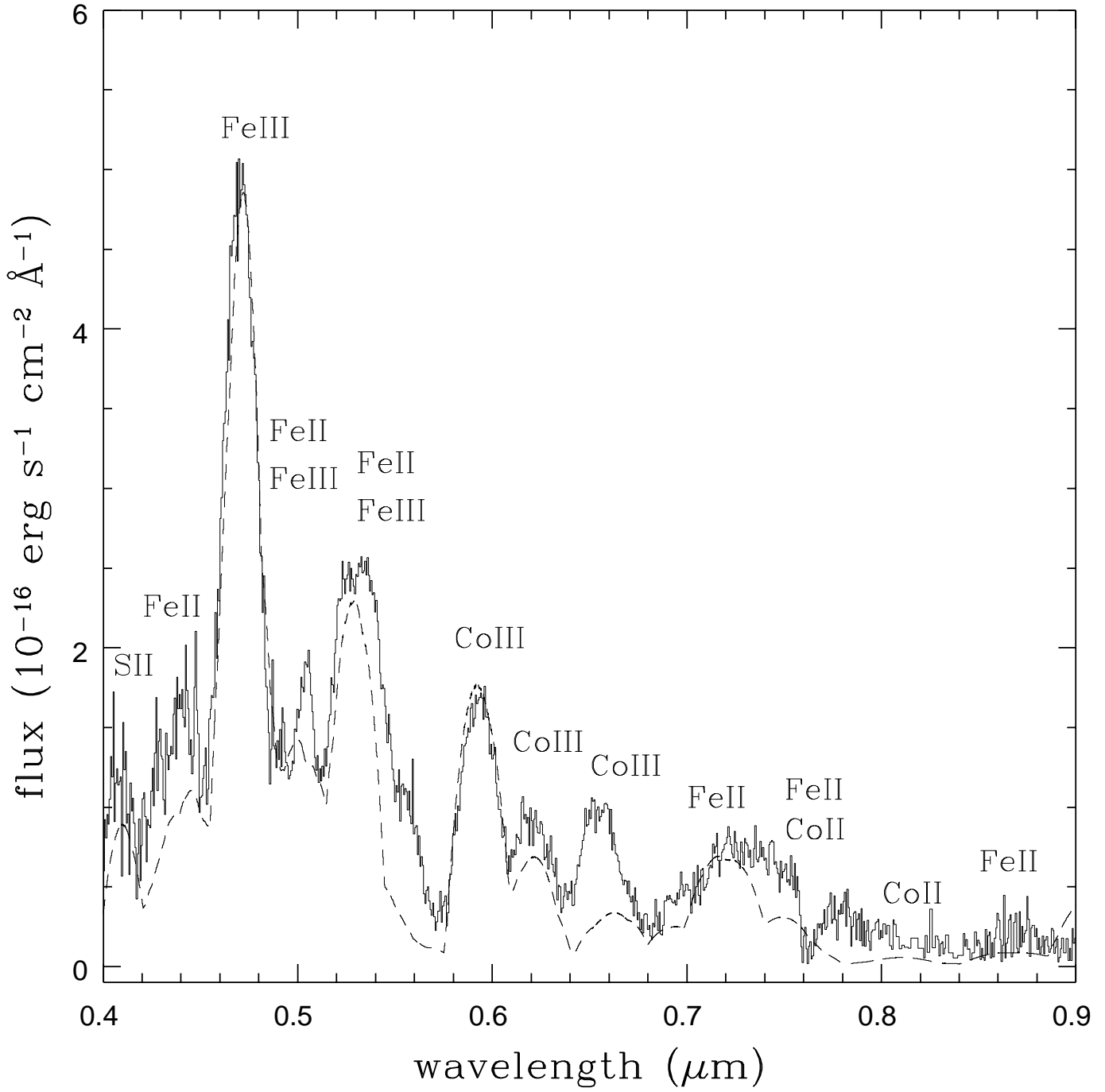
MODEL FIT OF SN 1995D AT 92-DAY EPOCH



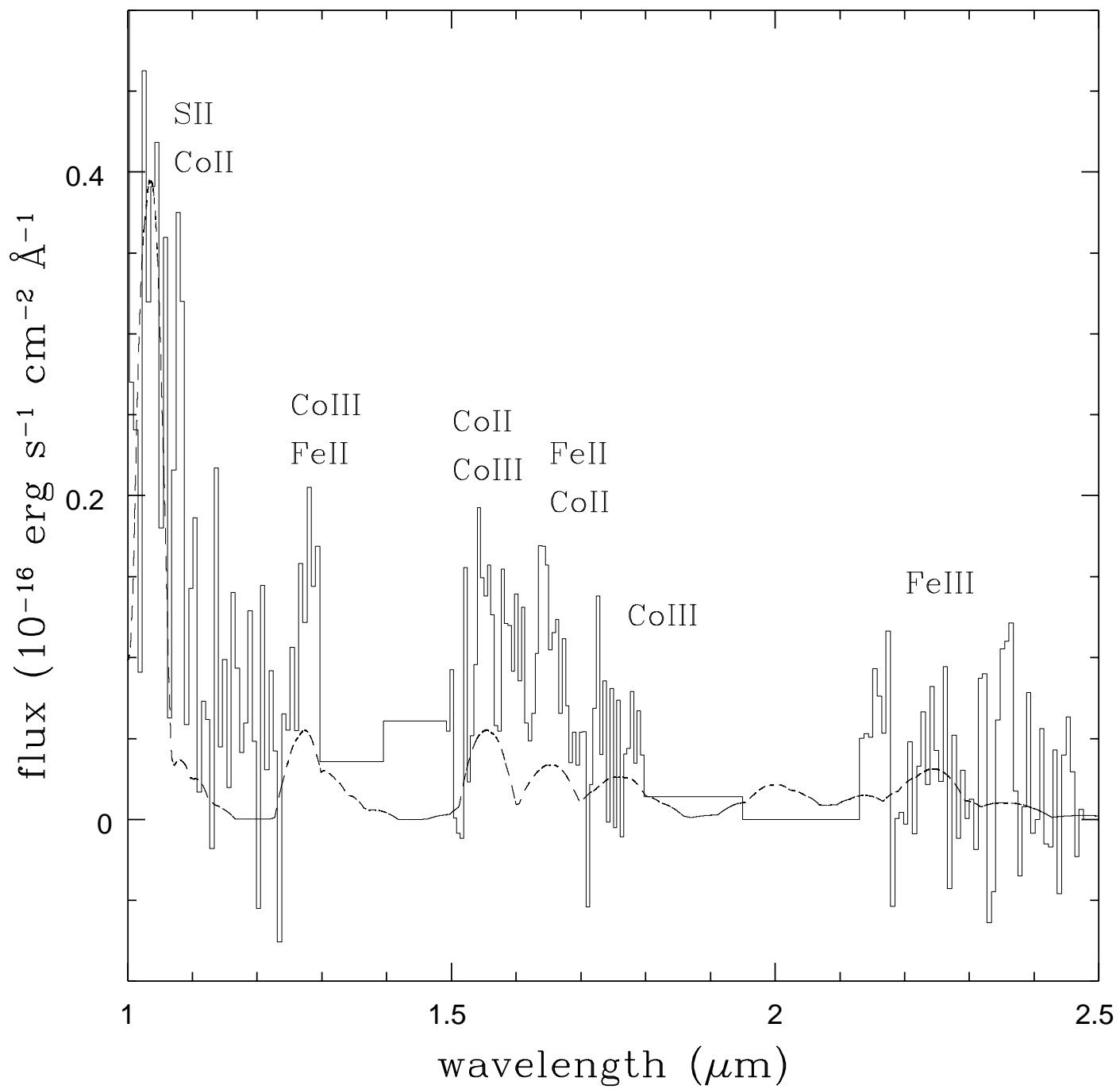
MODEL FIT OF SN 1995al AT 94-DAY EPOCH



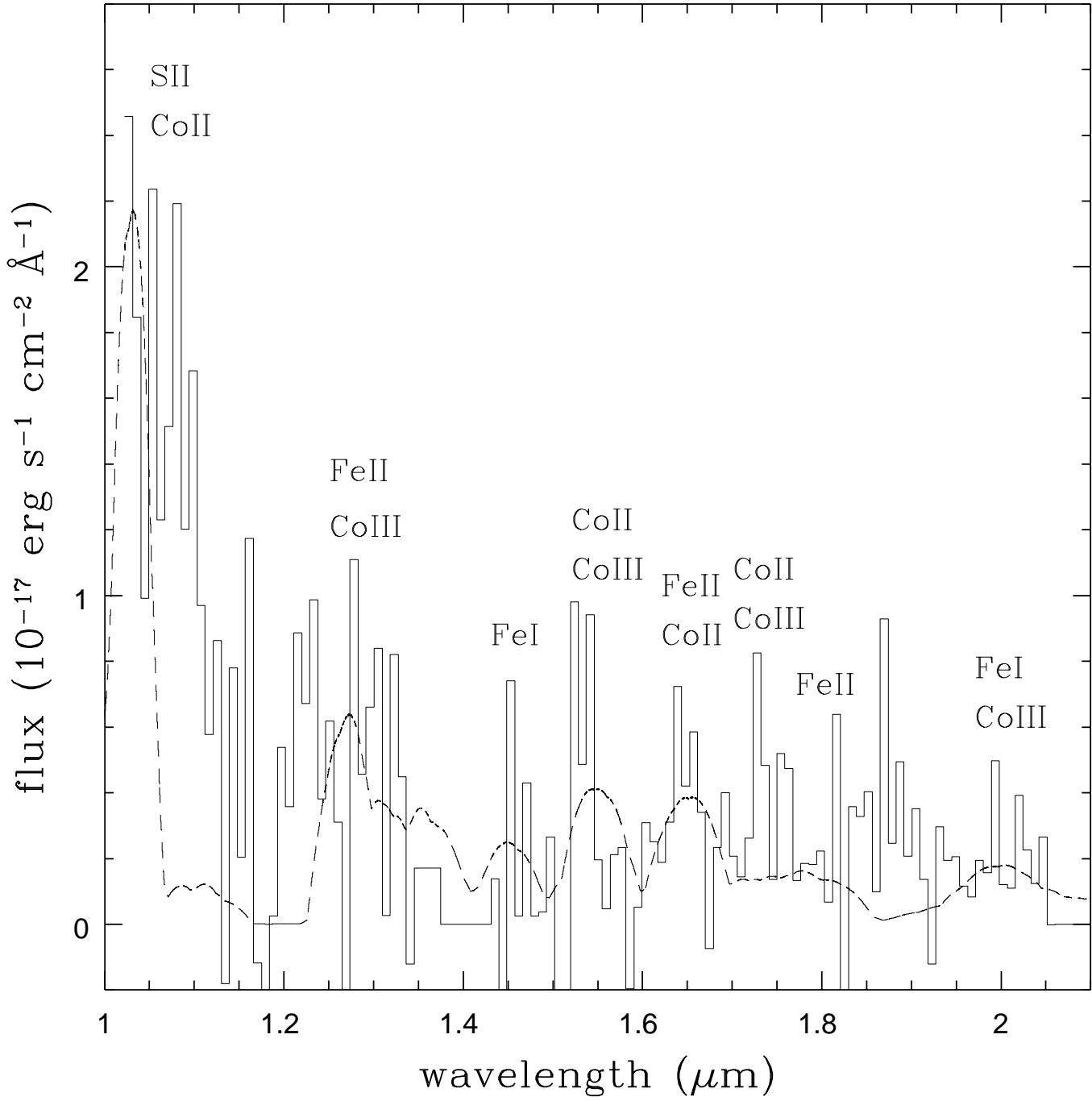
MODEL FIT OF SN 1995al AT 176-DAY EPOCH



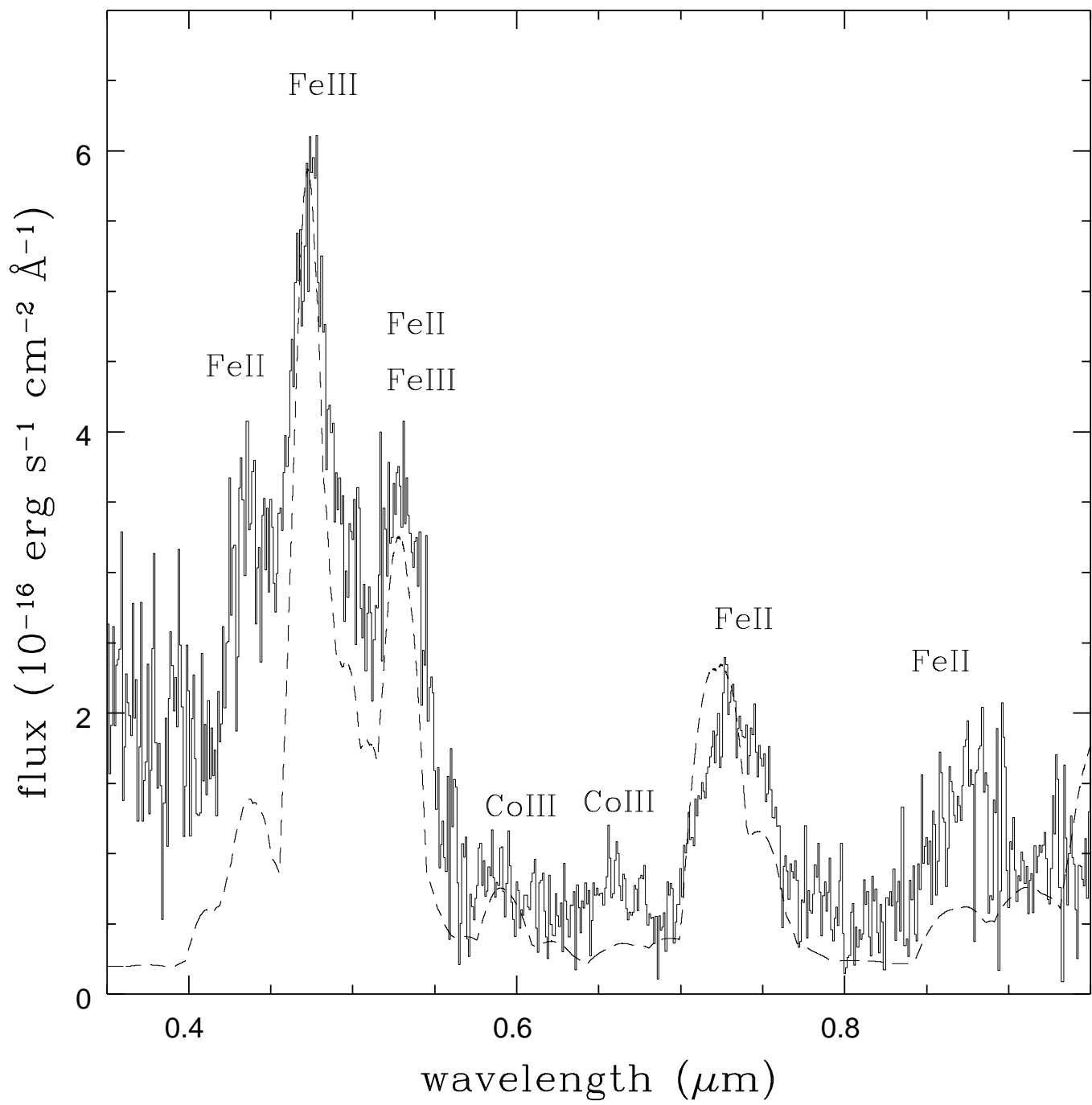
MODEL FIT OF SN 1995al AT 176-DAY EPOCH



MODEL FIT OF SN 1994ae AT 175-DAY EPOCH



MODEL FIT OF SN 1991T AT 338-DAY EPOCH



MODEL FIT OF SN 1991T AT 338-DAY EPOCH

